Nuclear Physics B105 (1976) 189–221

K^-p REACTIONS FROM 0.960 TO 1.355 GeV/c INVOLVING TWO-BODY FINAL STATES

Rutherford Laboratory – Imperial College Collaboration

B. CONFORTO *, G.P. GOPAL, G.E. KALMUS, P.J. LITCHFIELD, R.T. ROSS and A.J. VAN HORN
Rutherford Laboratory, Chilton, Didcot, Oxon, England

T.C. BACON, I. BUTTERWORTH, E.F. CLAYTON and R.M. WATERS
Imperial College, London, England

Received 14 August 1975

Data are presented from a high statistics bubble chamber experiment to study K^-p interactions in the c.m. energy range 1775 to 1957 MeV. For the reactions $K^-p \to K^-p$, $K^-p \to \bar{K}^0n$, $K^-p \to \Lambda\pi^0$ and $K^-p \to \Sigma^\pm\pi^\mp$ channel cross sections, differential cross sections and, where appropriate, polarisation distributions have been obtained. The channel cross sections for $K^-p \to \Sigma^0\pi^0$ are presented. In general the results are in agreement with those previously published although a significant discrepancy has been found in the $\Sigma^\pm\pi^\mp$ cross sections at the lower energies. New measurements of the $\Sigma^\pm$ lifetimes have also been obtained ($\tau_{\Sigma^-} = 1.49 \pm 0.03 \times 10^{-10}$ sec, $\tau_{\Sigma^+} = 0.807 \pm 0.013 \times 10^{-10}$ sec).

1. Introduction

The reactions

$$K^-p \to K^-p \quad (1)$$
$$\to \bar{K}^0n \quad (2)$$
$$\to \Lambda\pi^0 \quad (3)$$
$$\to \Sigma^-\pi^+ \quad (4)$$
$$\to \Sigma^+\pi^- \quad (5)$$

have been studied in the K^- momentum range 0.960 to 1.355 GeV/c corresponding to a c.m. energy range 1775 to 1957 MeV. The experimental procedures are discus-

* Present address: Istituto di Fisica dell' Universita, Piazzale delle Scienze 5, Rome, Italy.

sed. Additional details are given in ref. [1]. Cross sections and differential cross sections are given for these reactions, and polarisation distributions are presented for reactions (3) and (5). In addition cross sections are given for the reaction

$$K^-p \to \Sigma^0\pi^0 \,. \tag{6}$$

These data have been combined with published data in the energy range 1500 MeV to 2250 MeV for partial-wave analyses of the two-body $\bar{K}N$ reactions. These analyses will be presented elsewhere.

2. Exposure, scanning and measurements

Approximately 440 000 pictures were obtained in the CERN 2m Hydrogen Bubble Chamber, exposed to a separated K^- beam tuned to eleven equally spaced momentum settings between 1.000 and 1.400 GeV/c at the chamber entrance (corresponding to 0.960 and 1.360 GeV/c at the centre of the chamber). The average number of beam tracks per picture varied from 6 at the lowest momentum to 15 at the highest. The momentum bite was typically ±1%.

All frames were scanned for events of any topology except one prongs (predominantly beam decays) and zero prongs with no visible neutral decays. A restricted fiducial volume was imposed in order to ensure a high scanning efficiency and to mi-

Table 1
The numbers of events by topology found at each momentum setting

Beam momentum at chamber entrance (GeV/c)	Topology [a] 001	200	210	300
1.00	3730	13610	3186	1302
1.04	3844	12870	3128	1134
1.08	6217	22081	5297	1754
1.12	5597	20359	5090	1670
1.16	5245	21869	5012	1843
1.20	5248	24126	5378	2073
1.24	4486	22280	4874	1885
1.28	5515	27448	6178	2592
1.32	5240	27458	6312	2559
1.36	5221	27934	6474	2613
1.40	6443	33442	7617	3192
Total	56786	253477	58546	22617

[a] An event with I charged outgoing particles from the production vertex, J charged decays and K neutral decays is assigned the topology IJK.

nimize reconstruction problems. In order to determine scanning efficiencies a quarter of the film was scanned independently a second time and discrepancies between the two scans were resolved by a check scan. The scanning efficiencies were typically 96% for a single scan and greater than 99% for double scan. A total of approximately 494 000 events were measured using the Rutherford Laboratory HPD flying spot digitiser. The events were processed through the Rutherford Laboratory geometry and kinematics programmes [2]. Events that failed the first attempt were remeasured. If more than one hypothesis fitted a given event, the track ionisations measured by the HPD were compared with those predicted. Events still unresolved were inspected at the scanning table. Successful fits were summarised on a Data Summary Tape (DST). For the two-body channels presented here no ambiguity problems remain. Table 1 gives the number of events of each topology on the DST's for each momentum setting. (An event with I charged outgoing particles from the production vertex, J charged decays and K neutral decays is assigned the topology IJK.)

3. Beam calibration and cross section normalisation

The average beam momentum at each momentum setting was determined from four constraint (4C) kinematic fits to τ decays ($K^- \to \pi^+\pi^-\pi^-$). The beam momentum used for kinematic fitting was a weighted mean of this average momentum and the measured momentum for the event. Appropriate cuts were applied to the position and direction of the beam track for each event on the DST's, including τ decays, to ensure a well defined beam at each momentum setting. There is a significant over-

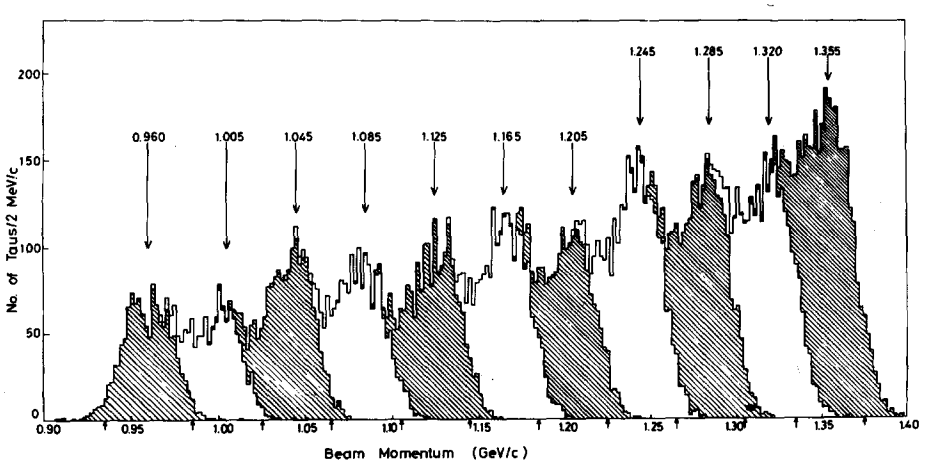

Fig. 1. The beam momentum distribution at the vertex from fitted τ decays. The final intervals chosen are indicated by arrows on the axis and the central values by arrows above. Alternate momentum settings are shaded.

Table 2
Microbarn equivalents for each beam momentum interval

Beam momentum at vertex (GeV/c) a)	c.m. energy (MeV)	No. of taus (after beam cuts)	Corrected total no. of taus	No. of events/μb
0.960	1775	1340	1517 ± 45	0.732 ± 0.022
1.005	1796	1134	1250 ± 39	0.631 ± 0.020
1.045	1815	1617	1857 ± 50	0.975 ± 0.026
1.085	1833	1525	1750 ± 49	0.954 ± 0.027
1,125	1852	1702	1870 ± 48	1.057 ± 0.027
1.165	1870	1970	2268 ± 56	1.327 ± 0.033
1.205	1889	1952	2262 ± 56	1.369 ± 0.034
1.245	1907	2483	2793 ± 60	1.747 ± 0.038
1.285	1925	2306	2948 ± 63	1.903 ± 0.041
1.320	1941	2088	2448 ± 58	1.624 ± 0.038
1.355	1957	2974	3419 ± 69	2.328 ± 0.047

a) Values given are at centre of the momentum interval. The spread is as indicated in fig. 1.

lap between the momentum ranges spanned by adjacent momentum settings due to the energy loss by ionisation as the beam traverses the chamber. For this reason the data from different beam momentum settings have been merged and binned according to the fitted beam momentum at the primary vertex. Fig. 1 shows the beam momentum distribution at the primary vertex from τ decays. The momentum intervals chosen for data presentation are indicated.

The K^- path length was calculated from the number of successfully fitted τ decays corrected for scanning and kinematical reconstruction losses. The microbarn equivalent is given by

$$\mu = (\text{number of taus}) \cdot P_K \cdot 5.024 \times 10^{-4} , \qquad (7)$$

where P_K is the K^- beam momentum in GeV/c. This relationship assumes a K^- lifetime of 1.237×10^{-8} sec., a decay branching ratio $(K^- \to \pi^-\pi^+\pi^-)/(K^- \to \text{all})$ of 0.0558, [3] and a hydrogen density of 0.0620 g/cm^3 corresponding to the operating conditions of the chamber. This agrees with the value obtained from a measurement of the range of a sample of 100 muons from stopping pions. The microbarn equivalent for each beam momentum interval is given in table 2, together with the numbers of τ's before and after corrections.

The normalisation has been checked by a measurement of the total beam track length at the first, sixth and eleventh momentum settings. The beam contamination was determined at these settings by a δ ray count and varies from 8% at the highest to 28% at the lowest momentum. The small number of fits to the reaction:

$$\pi^- p \to K^+ \Sigma^- \qquad \text{(topology 220)}$$

and the absence of fits to the reaction:

$$\pi^- p \to K^0 \Lambda \qquad \text{(topology 002)}$$

indicate that the pion contribution was less than 2% at all momenta, decreasing to less than $\frac{1}{2}$% at the highest momentum. Hence the contamination was predominantly muons.

4. Elastic scattering

Elastic scattering events (from 2-prongs including those with a decaying negative particle) were identified by 4C kinematic fits. Where an ambiguity occurred between the 4C and the corresponding 1C (π^0 production) fits, the former was preferred.

In a bubble chamber experiment elastic events suffer losses if the plane of the event is perpendicular to the chamber window or if the scattering angle is small. Losses of the first type were investigated as a function of r_p, the recoil proton range. The distribution of the angle ϕ between the normal to the scattering plane and an event dependent z axis ($\hat{z} = \hat{K}_{in} \times \hat{y}$, where $\hat{K}_{in}$ is the direction of the incident K^- and the xy plane is defined as the plane of the back of the front glass with the x axis along the length of the chamber), was examined for nine intervals of r_p. Losses were observed around $\phi = \frac{1}{2}\pi$. For each of these intervals events in the affected region were removed, and the remaining events were weighted. The fractions of the ϕ distributions removed are shown in fig. 2 as a function of r_p. For each interval of r_p the scanning efficiencies were determined from events outside the ϕ cuts. The single scan efficiency is shown in fig. 2.

Each event was assigned an overall weight

$$W = W_\phi \frac{1}{\epsilon_s \epsilon_t} , \tag{8}$$

where W_ϕ is the ϕ weight, ϵ_s is the scanning efficiency (for single or double scanned events as a function of r_p) and ϵ_t is the throughput efficiency, which is defined for a given class of events as the ratio of the number of events that reached the final DST to the number of events scanned. The total weighted number of elastic events at each incident momentum is shown in table 3 and the values of the differential cross section $d\sigma/d(\cos\theta)$ as a function of $\cos\theta$ are presented in table 4 and shown in fig. 3. The c.m. scattering angle θ is defined by: $\cos\theta = \hat{K}_{in} \cdot \hat{K}_{out}$ where $\hat{K}_{out}$ is the direction of the outgoing meson. The $\cos\theta$ distributions show a loss of events with small angle scatters ($\cos\theta > 0.975$). To estimate this loss the c.m. scattering angle distribution with $\cos\theta < 0.975$ was fitted by a Legendre polynomial expansion

$$\frac{d\sigma}{d(\cos\theta)} = 2\pi\lambda\!\!\!^{-2} \sum_{l=0}^{l_{max}} A_l P_l(\cos\theta) . \tag{9}$$

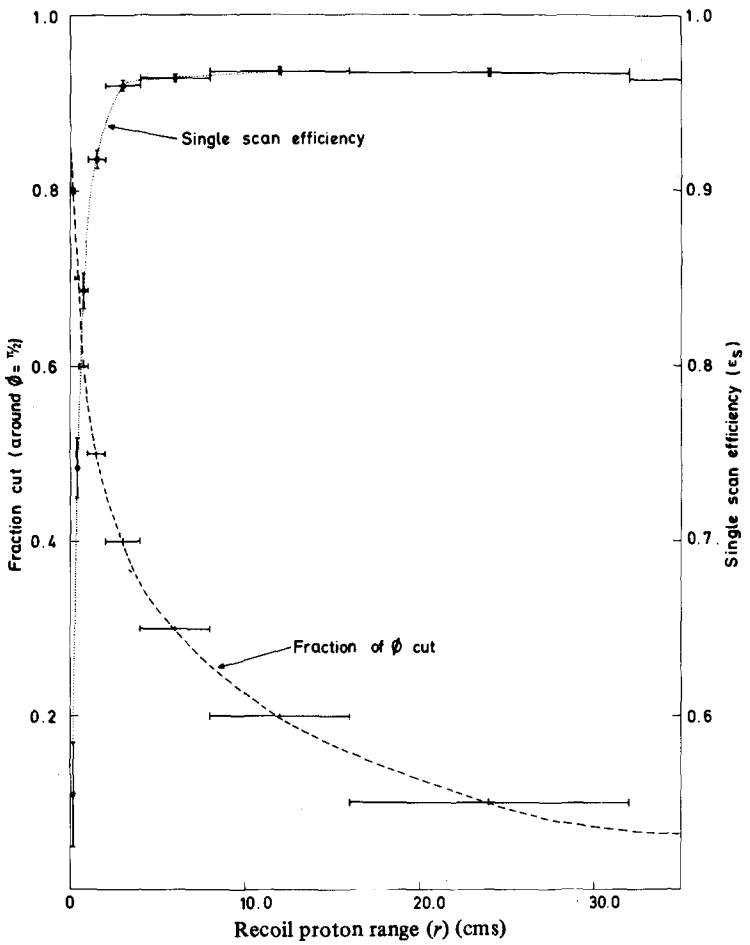

Fig. 2. The fraction of the ϕ distribution removed (indicated by the dashed curve) and the single efficiency (indicated by the dotted curve) as a function of the projected recoil proton range for elastic events.

The coefficients were determined by the minimum χ^2 method. At each energy, the maximum order of expansion (l_{max}) required was determined using the F-ratio [4] test, with the condition that the order should not decrease with increasing incident momentum. The number of events lost in the forward bin ($\cos\theta > 0.975$) was determined at each energy by extrapolation. The extrapolated values of $d\sigma/d(\cos\theta)$ at $\cos\theta = 1.0$ are given in table 4. The final corrected totals of elastic events are given in table 3 and the total elastic cross sections are given in table 17 and shown in fig. 10. When an additional term is included in the expansion, the total elastic cross sections are unchanged and the values of $d\sigma/d(\cos\theta)$ (at $\theta = 0$) are well within the er-

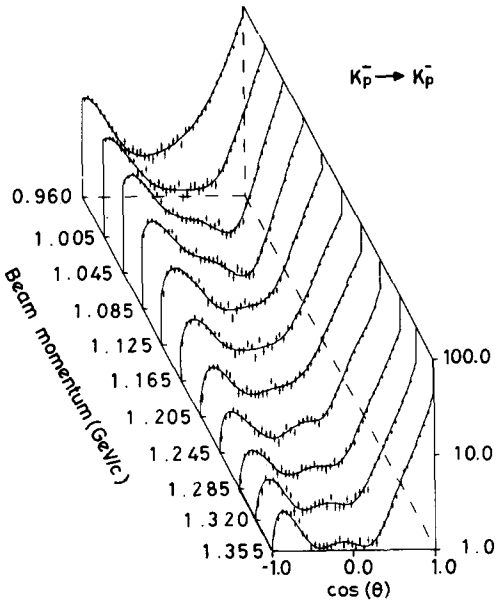

Fig. 3. Differential cross sections for elastic events. The curves are the results of the Legendre polynomial fits described. Vertical axis is $d\sigma/d(\cos\theta)$ in mb/unit $\cos\theta$.

rors quoted. The best Legendre polynomial expansion fits are shown superimposed on the data in fig. 3. The values of A_0 ($= \sigma_{\text{elastic}}/4\pi\lambda^2$) and the shape coefficients ($C_l = A_l/A_0$) are given in table 5. It should be noted that these coefficients are correlated and that the errors quoted are obtained from only the diagonal elements of the full error matrix.

5. The reactions $K^-p \rightarrow \bar{K}^0n$, $K^-p \rightarrow \Lambda\pi^0$ and $K^-p \rightarrow \Sigma^0\pi^0$

Events of 001 topology were fitted to reactions (2) and (3). The $\bar{K}^0n$ events were well separated but problems exist in separating the $\Lambda\pi^0$ from other Λ + neutral channels, as discussed below. Any kinematic ambiguities between Λ and K^0 fits to the V^0's are completely resolved by ionisation measurements. The neutral decay vertex was required to be within a restricted fiducial volume to ensure well-measured outgoing tracks. The biases were corrected as follows:

(a) *Missing mass squared.* A cut on the missing mass squared to the $\bar{K}^0$ (chosen as $0.683 \leqslant MM^2 \leqslant 1.083$) was sufficient to isolate the $\bar{K}^0n$ events. The distribution of missing mass squared to the Λ, shown in fig. 4, indicates substantial background on the high mass side of the π^0 peak (mainly from the channels $\Sigma^0\pi^0$ and $\Lambda\pi^0\pi^0$). To obtain angular distributions for $\Lambda\pi^0$ a missing mass squared cut of the form:

$$m_\pi^2 - 0.050 \leqslant MM^2 \leqslant m_\pi^2 + 0.050\,,$$

Table 3
The K^-p elastic events

Beam momentum (GeV/c) at vertex	No. of events after beam and vertex cuts	No. of events after ϕ cuts	Weighted no. of events excluding forward loss	Weighted no. of events including estimated forward loss
0.960	12167	10990	14981	15571 ± 167
1.005	10843	9723	13251	13727 ± 156
1.045	16771	15032	20579	21665 ± 197
1.085	14908	13356	18293	18914 ± 182
1.125	15288	13857	18373	18905 ± 178
1.165	16585	15235	19852	20424 ± 183
1.205	15356	14074	18228	19014 ± 176
1.245	17199	15900	20458	21518 ± 197
1.285	16784	15559	19964	20862 ± 193
1.320	13295	12325	15996	16660 ± 174
1.355	17838	16300	21393	22182 ± 201

Table 4
Differential cross section $d\sigma/d(\cos\theta)$ in (mb/unit $\cos\theta$) for $K^-p \to K^-p$

$\cos\theta$ bin centre		Beam momentum (GeV/c)										
		0.960	1.005	1.045	1.085	1.125	1.165	1.205	1.245	1.285	1.320	1.355
−0.975		10.82	10.71	9.35	5.97	3.46	2.50	1.57	1.42	1.25	1.50	1.55
	±	0.58	0.62	0.47	0.38	0.27	0.21	0.16	0.14	0.12	0.14	0.12
−0.925		11.49	11.14	10.37	8.39	5.67	4.01	2.64	2.35	2.21	1.97	2.20
	±	0.60	0.63	0.49	0.45	0.35	0.26	0.21	0.17	0.16	0.17	0.15
−0.875		10.51	11.03	11.08	8.56	6.59	4.15	3.28	2.48	2.38	2.79	2.58
	±	0.57	0.63	0.51	0.45	0.38	0.26	0.23	0.18	0.17	0.20	0.16
−0.825		9.51	10.06	10.50	8.17	6.08	4.67	3.31	2.85	2.43	2.50	2.55
	±	0.55	0.60	0.49	0.44	0.36	0.28	0.23	0.19	0.17	0.19	0.16
−0.775		7.96	8.55	9.07	7.62	6.22	3.93	3.33	2.69	2.44	2.63	2.46
	±	0.50	0.55	0.46	0.43	0.36	0.26	0.23	0.19	0.17	0.19	0.15
−0.725		7.07	8.20	8.46	6.57	5.73	4.36	2.69	2.29	2.51	2.35	1.92
	±	0.47	0.54	0.44	0.40	0.35	0.27	0.21	0.17	0.17	0.18	0.14
−0.675		5.85	6.55	7.47	6.49	5.50	3.60	2.93	2.39	2.27	1.93	2.08
	±	0.43	0.48	0.42	0.39	0.34	0.25	0.22	0.18	0.16	0.16	0.14
−0.625		5.26	6.31	6.43	6.55	5.10	3.17	2.73	2.01	2.02	2.13	1.53
	±	0.40	0.47	0.39	0.40	0.33	0.23	0.21	0.16	0.15	0.17	0.12
−0.575		4.57	4.78	6.82	5.62	4.38	3.10	2.24	1.66	1.67	1.81	1.40
	±	0.38	0.41	0.40	0.37	0.30	0.23	0.19	0.15	0.14	0.16	0.12
−0.525		3.51	4.69	5.71	4.21	4.68	3.04	1.75	1.57	1.42	1.22	1.06
	±	0.33	0.41	0.36	0.32	0.32	0.23	0.17	0.14	0.13	0.13	0.10
−0.475		3.86	5.17	4.41	4.20	3.72	2.38	1.82	1.74	1.61	1.43	1.17
	±	0.35	0.43	0.32	0.32	0.28	0.20	0.17	0.15	0.14	0.14	0.11
−0.425		3.01	3.72	4.39	3.97	2.75	2.34	1.95	1.56	1.42	1.21	1.12
	±	0.31	0.36	0.32	0.31	0.24	0.20	0.18	0.14	0.13	0.13	0.10
−0.375		3.17	3.41	4.55	3.73	3.00	2.29	1.75	1.55	1.43	1.26	1.12
	±	0.31	0.35	0.32	0.30	0.25	0.20	0.17	0.14	0.13	0.13	0.10
−0.325		2.85	3.73	4.09	4.07	2.59	1.87	1.71	1.41	1.37	1.29	1.10
	±	0.30	0.36	0.31	0.31	0.23	0.18	0.17	0.13	0.13	0.13	0.10
−0.275		2.91	3.32	3.68	3.21	2.59	2.03	1.71	1.25	1.35	1.43	1.08
	±	0.30	0.34	0.29	0.28	0.23	0.18	0.17	0.13	0.13	0.14	0.10

Table 4 (continued)

−0.225		2.63	2.96	3.52	3.26	2.29	2.06	1.71	1.50	1.67	1.48	1.21
	±	0.29	0.33	0.29	0.28	0.22	0.19	0.17	0.14	0.14	0.14	0.11
−0.175		2.59	3.20	3.73	3.26	2.63	2.43	1.73	1.82	1.64	1.56	1.31
	±	0.28	0.34	0.29	0.28	0.24	0.20	0.17	0.15	0.14	0.15	0.11
−0.125		2.46	3.21	3.57	3.21	1.91	2.27	2.32	1.70	1.61	1.36	1.13
	±	0.28	0.34	0.29	0.28	0.20	0.20	0.20	0.15	0.14	0.14	0.10
−0.075		2.92	3.66	3.48	3.32	2.30	1.76	2.05	1.60	1.81	1.70	1.25
	±	0.30	0.36	0.28	0.28	0.22	0.17	0.18	0.14	0.15	0.15	0.11
−0.025		3.35	2.66	3.27	2.94	2.54	2.65	1.85	2.04	1.63	1.34	1.18
	±	0.32	0.31	0.28	0.26	0.23	0.21	0.17	0.16	0.14	0.14	0.11
0.025		2.78	2.85	3.72	2.78	2.81	1.98	2.00	2.13	1.64	1.32	1.04
	±	0.29	0.32	0.29	0.26	0.24	0.18	0.18	0.17	0.14	0.14	0.10
0.075		3.31	3.38	3.04	2.35	2.57	2.31	2.19	2.24	1.52	1.36	1.26
	±	0.32	0.35	0.27	0.24	0.23	0.20	0.19	0.17	0.13	0.14	0.11
0.125		3.85	3.46	3.07	2.12	2.48	2.18	2.09	2.23	1.67	1.62	1.05
	±	0.34	0.35	0.27	0.22	0.23	0.19	0.19	0.17	0.14	0.15	0.10
0.175		4.20	3.06	3.39	2.64	2.60	2.71	2.43	2.12	1.91	1.43	1.28
	±	0.36	0.33	0.28	0.25	0.23	0.21	0.20	0.17	0.15	0.14	0.11
0.225		3.51	3.29	2.67	2.44	2.83	2.97	2.78	1.94	1.74	1.74	1.22
	±	0.33	0.34	0.25	0.24	0.24	0.23	0.21	0.16	0.14	0.16	0.11
0.275		5.05	3.76	2.44	2.28	2.77	2.63	2.67	2.41	1.89	1.90	1.18
	±	0.40	0.37	0.24	0.23	0.24	0.21	0.21	0.18	0.15	0.16	0.11
0.325		5.20	3.63	2.54	2.23	3.25	3.49	3.16	2.48	2.45	2.02	1.53
	±	0.40	0.36	0.24	0.23	0.26	0.24	0.23	0.18	0.17	0.17	0.12
0.375		5.31	3.45	2.78	2.28	3.49	3.59	3.55	2.96	2.73	2.04	1.89
	±	0.41	0.35	0.25	0.23	0.27	0.25	0.24	0.19	0.18	0.17	0.14
0.425		6.17	4.78	3.15	3.20	3.64	4.57	4.35	3.85	2.95	2.99	2.39
	±	0.44	0.41	0.27	0.28	0.28	0.28	0.27	0.22	0.19	0.20	0.15
0.475		7.37	5.13	3.42	3.97	4.74	5.01	4.91	4.61	3.98	3.65	2.91
	±	0.48	0.43	0.28	0.31	0.32	0.29	0.28	0.24	0.22	0.23	0.17
0.525		8.34	6.24	5.10	5.23	6.35	6.63	6.75	5.71	4.96	4.41	3.59
	±	0.51	0.47	0.34	0.35	0.37	0.33	0.33	0.27	0.24	0.25	0.19
0.575		10.01	8.15	6.33	6.75	7.97	7.66	7.95	7.10	6.31	5.82	4.94
	±	0.56	0.54	0.38	0.40	0.41	0.36	0.36	0.30	0.27	0.28	0.22
0.625		12.48	10.25	9.44	8.96	11.46	10.71	9.95	9.13	8.15	6.92	6.79
	±	0.62	0.60	0.47	0.46	0.49	0.42	0.40	0.34	0.31	0.31	0.26
0.675		15.70	13.71	12.45	12.80	13.16	13.22	12.57	11.11	9.86	8.03	7.46
	±	0.70	0.70	0.54	0.55	0.53	0.47	0.45	0.38	0.34	0.33	0.27
0.725		18.89	18.55	17.55	17.28	18.16	16.34	15.35	13.97	12.02	10.30	9.59
	±	0.77	0.81	0.64	0.64	0.62	0.52	0.50	0.42	0.38	0.38	0.31
0.775		24.60	23.45	22.60	21.72	21.69	20.62	18.26	16.34	14.40	13.86	12.58
	±	0.92	0.96	0.75	0.73	0.68	0.59	0.55	0.46	0.41	0.44	0.35
0.825		31.12	32.11	32.56	32.26	27.86	24.73	23.19	19.76	18.46	16.86	15.71
	±	1.07	1.15	0.92	0.93	0.81	0.68	0.64	0.52	0.48	0.49	0.39
0.875		36.58	42.93	43.28	39.01	35.96	31.21	28.66	24.90	22.20	20.96	20.34
	±	1.23	1.41	1.13	1.08	0.97	0.80	0.75	0.61	0.55	0.58	0.47
0.925		50.92	54.59	61.28	55.46	47.66	38.38	36.37	32.66	27.85	27.56	27.88
	±	1.62	1.77	1.49	1.42	1.23	0.97	0.93	0.77	0.68	0.72	0.61
0.9625		63.37	68.14	77.84	64.33	56.44	49.10	42.98	37.60	35.80	34.63	32.45
	±	3.20	3.41	2.93	2.64	2.28	1.86	1.70	1.38	1.27	1.35	1.08
1.000 [a]		73.93	83.23	93.36	80.25	65.08	53.74	49.32	48.84	41.82	41.53	41.95
	±	3.44	3.85	3.40	3.15	2.55	2.06	1.91	2.23	1.99	2.12	1.73

[a] The forward differential cross section is the extrapolated value of the Legendre polynomial fit.

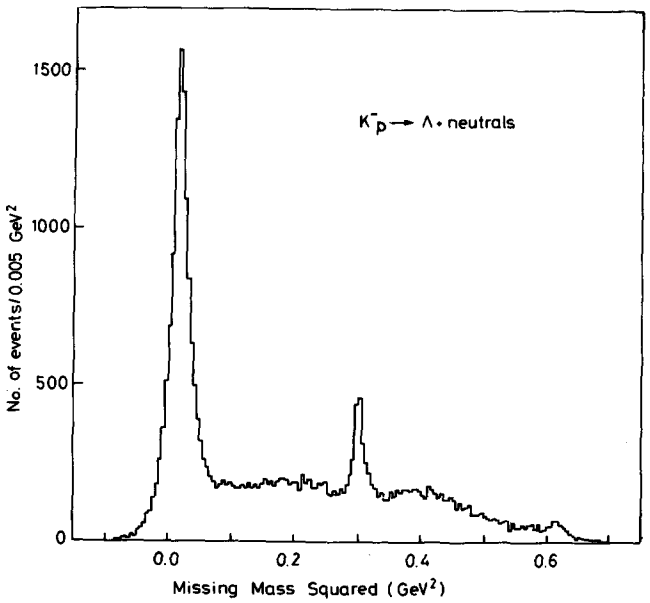

Fig. 4. The distribution of the missing mass squared to the Λ from events of the type $K^-p \to \Lambda$ + neutrals.

Table 5
Values of A_0 ($= \sigma/4\pi\lambda^2$) and the shape coefficients ($C_l = A_l/A_0$) for $K^-p \to K^-p$

Beam momentum (GeV/c)		A_0	C_1	C_2	C_3	C_4	C_5	C_6	C_7	C_8	C_9
0.960		1.120	1.233	2.002	1.114	0.861	0.506	0.123	0.112		
	±	0.036	0.027	0.038	0.045	0.049	0.050	0.041	0.037		
1.005		1.226	1.223	2.144	1.431	1.049	0.596	0.115	0.093		
	±	0.041	0.029	0.041	0.048	0.051	0.051	0.042	0.039		
1.045		1.326	1.235	2.222	1.721	1.205	0.751	0.127	0.141		
	±	0.037	0.023	0.033	0.039	0.041	0.040	0.033	0.030		
1.085		1.249	1.332	2.183	1.718	1.051	0.630	0.069	0.112		
	±	0.037	0.025	0.035	0.041	0.044	0.042	0.035	0.032		
1.125		1.189	1.436	2.050	1.523	0.764	0.524	−0.025	0.007		
	±	0.032	0.024	0.034	0.040	0.043	0.042	0.036	0.031		
1.165		1.074	1.549	1.956	1.383	0.678	0.395	−0.027	0.049		
	±	0.028	0.022	0.032	0.037	0.041	0.040	0.035	0.029		
1.205		1.017	1.664	1.947	1.381	0.687	0.382	−0.024	0.066		
	±	0.027	0.023	0.032	0.038	0.043	0.041	0.036	0.029		
1.245		0.944	1.698	1.969	1.422	0.772	0.458	0.094	0.220	0.172	0.125
	±	0.022	0.023	0.034	0.041	0.048	0.051	0.052	0.048	0.041	0.031
1.285		0.878	1.671	1.967	1.436	0.737	0.415	0.053	0.183	0.120	0.048
	±	0.021	0.024	0.034	0.042	0.048	0.052	0.053	0.049	0.041	0.032
1.320		0.853	1.666	2.063	1.546	0.875	0.545	0.111	0.212	0.078	−0.000
	±	0.022	0.027	0.038	0.047	0.055	0.058	0.060	0.055	0.046	0.036
1.355		0.822	1.717	2.221	1.674	1.014	0.615	0.157	0.274	0.095	0.038
	±	0.018	0.023	0.034	0.041	0.048	0.051	0.052	0.048	0.039	0.030

where m_π is the π^0 mass ($m_\pi^2 = 0.018$ GeV^2) was applied. This eliminated essentially all the multi-π^0 background. The remaining events were weighted by the inverse of the probability P that their missing mass would satisfy this cut.

$$P = \frac{1}{\sqrt{2\pi}\sigma} \int_{-0.032}^{0.068} \exp\left[-\frac{(MM^2 - m_\pi^2)^2}{2\sigma^2}\right] dMM^2 , \tag{10}$$

where σ is the error in the missing mass squared for the particular event. (This method ignores the problem of $\Sigma^0\pi^0$ contamination which is discussed below.)

(b) *Lifetime weights.* A minimum length cut ($l_{\min}$) of 0.4 cm was applied to the decay length projected on the xy plane and the remaining events were weighted by the inverse of the probability that an event of that type would decay in the fiducial volume:

$$P = \exp(-l_1/\bar{l}) - \exp(-l_2/\bar{l}) , \tag{11}$$

where: $l_1 = l_{\min}/\cos\lambda$, λ being the dip of the V^0 with respect to the xy plane, l_2 = the potential decay length from the production vertex to the edge of the decay volume and $\bar{l} = pc\tau/M$ with $\tau(K^0) = 0.866 \times 10^{-10}$ sec. and $\tau(\Lambda) = 2.61 \times 10^{-10}$ sec. [3b].

(c) *Short decay tracks.* Losses of V^0's due to short decay tracks were corrected by imposing minimum momentum cuts, corresponding to cuts in the cos δ distribution, where δ is the angle between the decay track in the rest frame of the V^0 and the direction of the V^0. For Λ's the cuts chosen were 54 MeV/c for the pion, 140 MeV/c for the proton and for the K^0's 44 MeV/c for each pion. A weight

$$W = 2/(1 - \cos\delta_1) , \tag{12}$$

was applied to the remaining events, where δ_1 is the value of δ corresponding to the momentum cut off on the relevant decay track for a V^0 of the observed momentum.

(d) *Decay angle losses.* A weight was applied to correct for a small loss of $\bar{K}^0$ events when the decay plane was perpendicular to the chamber window. There is also a small loss of events in which the $\bar{K}^0$ is produced backward with respect to the beam direction in the laboratory. This was corrected by applying an empirical weight depending on the position of the event and on the production angle in the chamber. For Λ's no such losses were observed.

(e) $\Sigma^0\pi^0$ *background.* In the $\Lambda\pi^0$ channel the missing mass squared cut did not exclude all the $\Sigma^0\pi^0$ background, which has a flat missing mass squared spectrum extending from a value slightly above m_π^2 to an upper limit near 0.3 GeV^2. A cut that included only those events with missing mass squared less than m_π^2 would have eliminated these background events but would have lost 50% of the genuine $\Lambda\pi^0$ events. Hence a small number of $\Sigma^0\pi^0$ events still remain in our data, and they present a possible source of bias in our angular distributions. We have estimated the amount of contamination present by examining the asymmetry of the MM^2 distribution about m_π^2 and have concluded that 5 ± 2% of the events in our angular distri-

Table 6(a)
The $\bar{K}^0 n$ events

Beam momentum (GeV/c)	No. of events after beam cuts	No. of events after all cuts	Weighted no. of events
0.960	1251	1007	1599 ± 51
1.005	1331	1065	1632 ± 51
1.045	2266	1866	2907 ± 68
1.085	2010	1671	2574 ± 64
1.125	1802	1461	2186 ± 58
1.165	1621	1330	2017 ± 56
1.205	1273	1047	1603 ± 50
1.245	1224	1001	1524 ± 49
1.285	1074	884	1365 ± 47
1.320	782	641	988 ± 40
1.355	1171	955	1444 ± 47

Table 6(b)
The $\Lambda\pi^0$ events

Beam momentum (GeV/c)	No. of events after beam cuts	No. of events after all cuts	Weighted no. of events
0.960	1518	1227	1600 ± 69
1.005	1267	1003	1285 ± 65
1.045	1560	1205	1518 ± 67
1.085	1237	958	1231 ± 60
1.125	1263	956	1224 ± 58
1.165	1267	981	1258 ± 59
1.205	1203	933	1202 ± 56
1.245	1471	1158	1499 ± 62
1.285	1322	1059	1346 ± 59
1.320	1035	783	987 ± 50
1.355	1781	1406	1785 ± 79

butions and polarisation distributions are from this background. These distributions would be biased by such a background only if the $\Sigma^0\pi^0$ angular distributions were extremely non-uniform. The presence of this contamination has been accounted for in calculating $\Lambda\pi^0$ cross sections as indicated below.

Throughput and scanning efficiencies were included in the final weight for each event. The throughput efficiency, ϵ_t, was typically 91% for the 001 topology. Numbers of events remaining after the cuts together with final weighted numbers of events are shown in table 6. The angular distributions, given in table 7 and shown in fig. 5, were fitted by the Legendre polynomial expansion of eq. (9). The maximum

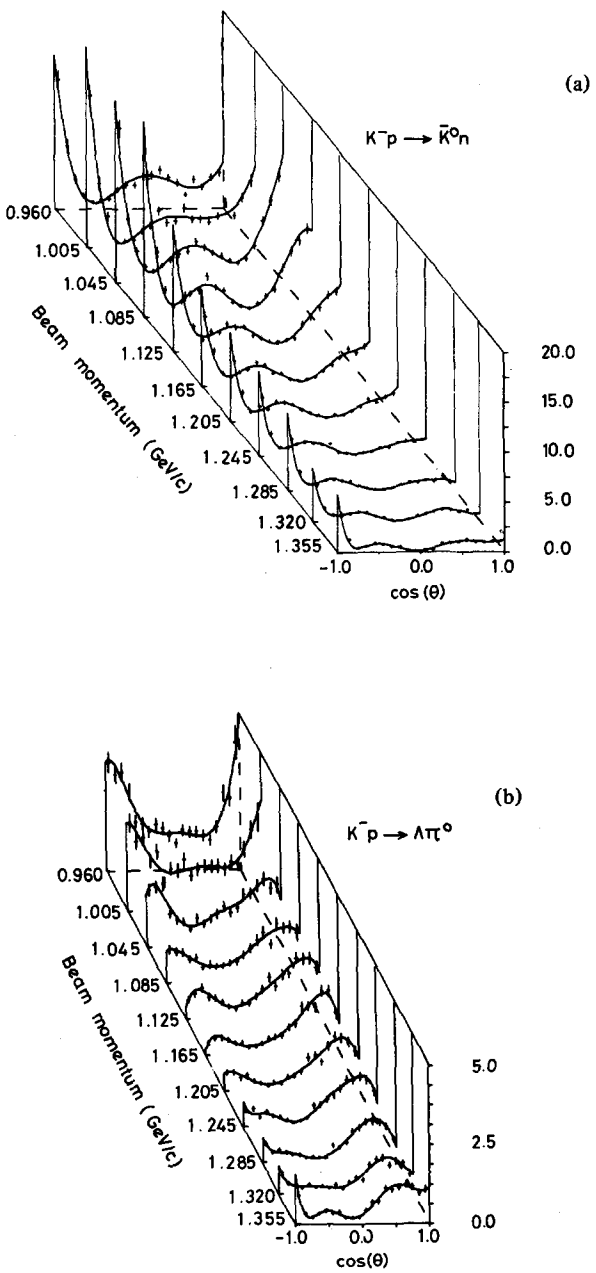

Fig. 5. Differential cross sections for (a) $K^-p \rightarrow \bar{K}^0n$, (b) $K^-p \rightarrow \Lambda\pi^0$. The curves are the results of the Legendre polynomial fits described. Vertical axis is $d\sigma/d(\cos\theta)$ in mb/unit $\cos\theta$.

Table 7
Differential cross section $d\sigma/d(\cos\theta)$ (mb/unit $\cos\theta$)
(a) $K^-p \to \bar{K}^0 n$

$\cos\theta$ bin centre		Beam momentum (GeV/c)										
		0.960	1.005	1.045	1.085	1.125	1.165	1.205	1.245	1.285	1.320	1.355
−0.950		13.20	15.43	15.67	14.02	9.50	7.04	6.23	5.98	5.19	3.62	3.78
	±	1.01	1.16	0.95	0.91	0.70	0.54	0.49	0.42	0.38	0.35	0.29
−0.850		6.41	6.55	6.44	6.61	5.63	3.60	2.95	2.31	1.95	1.31	1.31
	±	0.71	0.77	0.61	0.63	0.53	0.38	0.35	0.27	0.23	0.22	0.17
−0.750		3.05	3.20	3.18	2.79	2.57	1.33	0.92	0.89	0.72	0.68	0.40
	±	0.49	0.50	0.44	0.40	0.36	0.24	0.19	0.16	0.14	0.15	0.10
−0.650		1.44	0.66	1.62	1.05	1.17	1.03	1.51	0.84	0.71	0.59	0.64
	±	0.32	0.24	0.29	0.23	0.23	0.21	0.25	0.15	0.14	0.14	0.12
−0.550		0.72	0.70	1.15	1.58	2.03	1.55	1.21	1.19	1.06	0.79	0.91
	±	0.22	0.24	0.24	0.28	0.32	0.24	0.21	0.18	0.16	0.16	0.14
−0.450		0.87	0.82	1.77	2.34	1.90	1.79	1.99	1.41	1.11	0.94	0.79
	±	0.23	0.25	0.30	0.34	0.28	0.25	0.26	0.19	0.16	0.16	0.12
−0.350		0.96	1.70	2.30	2.66	2.84	2.43	1.85	1.28	1.03	0.89	0.57
	±	0.24	0.35	0.33	0.36	0.35	0.29	0.25	0.18	0.15	0.16	0.10
−0.250		2.00	2.26	2.86	4.07	2.55	2.19	1.64	1.11	1.06	0.56	0.54
	±	0.35	0.40	0.37	0.44	0.33	0.27	0.23	0.17	0.16	0.12	0.10
−0.150		2.43	3.75	3.12	3.00	2.49	1.39	1.08	1.19	0.49	0.44	0.22
	±	0.39	0.51	0.38	0.37	0.32	0.21	0.18	0.17	0.10	0.11	0.06
−0.050		2.41	2.47	4.11	2.66	1.58	1.28	0.86	0.38	0.24	0.15	0.14
	±	0.38	0.41	0.43	0.35	0.25	0.20	0.16	0.09	0.07	0.06	0.05
0.050		3.31	2.65	3.49	1.55	1.31	0.70	0.58	0.33	0.15	0.05	0.28
	±	0.44	0.42	0.39	0.26	0.23	0.15	0.13	0.09	0.06	0.04	0.07
0.150		3.47	4.00	2.93	1.02	1.03	0.56	0.30	0.21	0.14	0.22	0.25
	±	0.45	0.51	0.36	0.21	0.20	0.13	0.09	0.07	0.05	0.07	0.07
0.250		4.01	2.86	2.63	0.85	1.02	0.74	0.59	0.31	0.31	0.59	0.89
	±	0.48	0.43	0.34	0.19	0.20	0.15	0.13	0.08	0.08	0.12	0.12
0.350		3.12	2.89	2.25	1.33	1.12	0.97	0.61	0.44	0.62	0.78	0.97
	±	0.42	0.43	0.31	0.24	0.20	0.17	0.13	0.10	0.11	0.14	0.13
0.450		2.66	2.54	1.99	2.12	1.25	1.48	1.01	0.84	0.92	0.99	1.00
	±	0.38	0.40	0.29	0.30	0.21	0.21	0.17	0.14	0.14	0.16	0.13
0.550		1.44	3.11	2.31	2.74	2.80	2.07	1.40	0.83	0.83	1.13	1.28
	±	0.28	0.45	0.31	0.34	0.32	0.25	0.20	0.13	0.13	0.17	0.15
0.650		2.99	4.59	3.69	4.92	3.41	2.90	2.15	1.24	1.08	1.15	0.95
	±	0.41	0.54	0.39	0.45	0.35	0.29	0.25	0.16	0.15	0.17	0.13
0.750		2.17	3.26	6.21	6.58	4.33	3.75	1.88	1.48	0.91	0.95	0.98
	±	0.34	0.45	0.51	0.52	0.40	0.33	0.23	0.18	0.14	0.15	0.13
0.850		3.14	5.05	8.26	7.66	5.62	3.36	2.45	1.47	1.42	1.14	1.10
	±	0.41	0.56	0.58	0.56	0.45	0.32	0.26	0.18	0.17	0.16	0.14
0.950		3.63	6.76	10.67	8.85	5.96	3.98	2.80	1.60	0.90	0.69	1.07
	±	0.44	0.65	0.66	0.60	0.46	0.34	0.28	0.19	0.13	0.13	0.13

order was fixed in the manner described for reaction (1). The values of A_l obtained are given in table 8.

The average polarisation of the Λ in each $\cos\theta$ bin was calculated as

Table 7 (continued)

(b) $K^-p \to \Lambda\pi^0$

cos θ bin centre		Beam momentum (GeV/c)										
		0.960	1.005	1.045	1.085	1.125	1.165	1.205	1.245	1.285	1.320	1.355
−0.950		3.48	2.83	1.80	1.06	0.60	0.39	0.59	0.52	0.59	0.59	0.93
	±	0.34	0.30	0.20	0.15	0.12	0.08	0.10	0.08	0.09	0.09	0.10
−0.850		3.10	2.22	1.91	0.98	0.80	0.52	0.59	0.55	0.32	0.31	0.34
	±	0.29	0.27	0.20	0.14	0.12	0.09	0.09	0.08	0.06	0.06	0.06
−0.750		3.17	2.34	2.01	0.94	0.97	0.54	0.40	0.28	0.38	0.25	0.22
	±	0.32	0.28	0.22	0.14	0.14	0.09	0.08	0.06	0.07	0.06	0.04
−0.650		2.55	1.59	1.05	0.75	0.66	0.48	0.48	0.45	0.33	0.17	0.35
	±	0.28	0.23	0.15	0.12	0.12	0.09	0.09	0.08	0.06	0.05	0.06
−0.550		1.56	1.88	0.84	0.79	0.63	0.35	0.29	0.31	0.22	0.27	0.43
	±	0.22	0.25	0.13	0.13	0.11	0.07	0.07	0.06	0.05	0.06	0.06
−0.450		1.49	0.91	0.78	0.48	0.52	0.37	0.22	0.29	0.22	0.19	0.35
	±	0.20	0.17	0.13	0.10	0.10	0.08	0.06	0.06	0.05	0.05	0.06
−0.350		1.24	1.33	0.55	0.55	0.38	0.23	0.14	0.18	0.13	0.23	0.40
	±	0.19	0.21	0.11	0.13	0.09	0.06	0.05	0.05	0.04	0.05	0.06
−0.250		1.46	1.27	0.89	0.49	0.30	0.25	0.24	0.09	0.16	0.15	0.21
	±	0.20	0.21	0.14	0.10	0.08	0.06	0.06	0.03	0.04	0.04	0.04
−0.150		1.34	1.60	0.71	0.55	0.49	0.33	0.21	0.15	0.14	0.26	0.21
	±	0.19	0.23	0.13	0.11	0.10	0.08	0.07	0.04	0.04	0.07	0.04
−0.050		1.09	1.10	0.84	0.62	0.47	0.50	0.40	0.24	0.11	0.14	0.22
	±	0.18	0.19	0.14	0.11	0.10	0.09	0.08	0.05	0.04	0.04	0.04
0.050		0.85	1.30	1.01	0.66	0.67	0.54	0.42	0.63	0.51	0.34	0.43
	±	0.16	0.21	0.16	0.12	0.12	0.09	0.08	0.10	0.08	0.07	0.07
0.150		1.27	1.40	1.27	0.87	0.91	0.60	0.57	0.65	0.45	0.49	0.68
	±	0.19	0.21	0.17	0.14	0.14	0.10	0.09	0.10	0.07	0.08	0.08
0.250		1.22	1.38	1.08	1.06	1.28	0.83	1.02	0.82	0.60	0.41	0.71
	±	0.19	0.22	0.15	0.15	0.16	0.12	0.13	0.10	0.08	0.07	0.08
0.350		1.22	1.39	1.22	1.32	0.98	0.94	1.08	0.93	0.94	0.88	1.14
	±	0.19	0.22	0.16	0.18	0.14	0.12	0.13	0.11	0.10	0.11	0.11
0.450		1.09	1.31	1.63	1.57	1.36	1.48	0.88	1.16	1.07	1.05	1.09
	±	0.18	0.21	0.19	0.19	0.17	0.16	0.12	0.12	0.11	0.12	0.10
0.550		0.92	1.53	1.65	1.19	1.40	1.49	1.36	1.44	1.24	1.11	1.17
	±	0.17	0.23	0.19	0.16	0.17	0.16	0.15	0.13	0.12	0.12	0.10
0.650		1.36	1.45	1.89	1.83	1.87	1.45	1.66	1.43	1.25	0.87	1.25
	±	0.20	0.22	0.21	0.20	0.19	0.15	0.16	0.13	0.12	0.11	0.11
0.750		2.44	1.93	2.11	1.69	1.83	1.97	1.62	1.53	1.22	0.99	1.18
	±	0.27	0.26	0.22	0.19	0.19	0.18	0.16	0.14	0.12	0.12	0.11
0.850		2.28	2.54	1.81	1.71	1.86	1.95	1.49	1.42	1.10	0.92	0.96
	±	0.26	0.30	0.20	0.20	0.20	0.18	0.15	0.13	0.11	0.11	0.10
0.950		4.07	2.93	1.93	1.52	1.56	1.25	1.21	1.05	0.68	0.60	1.08
	±	0.55	0.47	0.26	0.27	0.22	0.18	0.17	0.13	0.10	0.10	0.12

$$P(\cos\theta) = \sum_{i=1}^{N} (\cos\chi_i)/(\tfrac{1}{3}\alpha N)\,, \qquad (13)$$

where N is the number of unweighted events in the bin and $\alpha = 0.647$ is the Λ decay

Table 8(a)
Values of Legendre A_l coefficients (with $A_0 = \sigma/4\pi\lambda^2$) for $K^-p \to \bar{K}^0 n$

Beam momentum (GeV/c)	A_0	A_1	A_2	A_3	A_4	A_5	A_6	A_7	A_8	A_9
0.960	0.334	−0.151	0.338	−0.403	0.451	−0.075	−0.013			
	± 0.018	0.024	0.037	0.041	0.045	0.039	0.042			
1.005	0.424	−0.079	0.547	−0.443	0.616	−0.265	0.100			
	± 0.022	0.029	0.050	0.050	0.058	0.049	0.052			
1.045	0.517	0.018	0.734	−0.199	0.720	−0.354	−0.028	−0.119		
	± 0.024	0.027	0.051	0.044	0.057	0.055	0.050	0.055		
1.085	0.494	0.005	0.772	−0.169	0.514	−0.564	0.094	0.101		
	± 0.023	0.028	0.052	0.043	0.052	0.060	0.050	0.056		
1.125	0.399	−0.030	0.559	−0.113	0.329	−0.388	0.064	0.053		
	± 0.019	0.023	0.041	0.036	0.042	0.049	0.044	0.050		
1.165	0.308	−0.020	0.392	−0.110	0.195	−0.355	0.155	0.039		
	± 0.015	0.019	0.031	0.029	0.033	0.040	0.036	0.039		
1.205	0.249	−0.080	0.328	−0.094	0.193	−0.304	0.197	−0.011		
	± 0.012	0.018	0.028	0.028	0.031	0.036	0.033	0.035		
1.245	0.194	−0.124	0.287	−0.141	0.179	−0.283	0.179	−0.031	−0.020	0.017
	± 0.009	0.015	0.023	0.024	0.027	0.032	0.033	0.037	0.032	0.036
1.285	0.167	−0.118	0.246	−0.173	0.136	−0.263	0.176	−0.084	−0.054	0.038
	± 0.008	0.014	0.021	0.023	0.024	0.029	0.030	0.035	0.029	0.033
1.320	0.147	−0.057	0.173	−0.156	0.043	−0.178	0.154	−0.056	−0.061	−0.036
	± 0.008	0.013	0.019	0.023	0.023	0.028	0.031	0.035	0.030	0.035
1.355	0.156	−0.042	0.198	−0.181	0.100	−0.160	0.210	−0.097	−0.019	−0.023
	± 0.007	0.011	0.017	0.021	0.021	0.024	0.027	0.031	0.027	0.030

asymmetry parameter [3]. The angle χ is defined by $\cos\chi = \hat{p}\cdot\hat{n}$ where $\hat{p}$ is the direction of the decay proton in the Λ rest frame and $\hat{n}$ is the normal to the production plane.

$$\hat{n} = (\hat{K}_{in} \times \hat{\pi}^0)/|\hat{K}_{in} \times \hat{\pi}^0| .$$

The error ΔP is given by

$$\Delta P = [(3 - Q)/\alpha^2 N]^{1/2} , \tag{14}$$

where $Q = (\alpha P)^2$ or 1, whichever is smaller.

These $\cos\theta$ bins were chosen to have at least 40 events per bin. The resulting polarisation distributions are listed in table 9 and shown in fig. 6. The $\underset{\sim}{P}\mathrm{d}\sigma/\mathrm{d}(\cos\theta)$ distributions were fitted by an associated Legendre polynomial fit of the form:

$$\underset{\sim}{P}\frac{\mathrm{d}\sigma}{\mathrm{d}(\cos\theta)} = 2\pi\lambda^2\hat{n}\sum_{l=1}^{l_{max}} B_l P_l^1(\cos\theta) . \tag{15}$$

Table 8(b)
Values of Legendre A_l coefficients (with $A_0 = \sigma/4\pi\lambda^2$) for $K^-p \to \Lambda\pi^0$

Beam momentum (GeV/c)	A_0	A_1	A_2	A_3	A_4	A_5	A_6	A_7	A_8	A_9
0.960	0.196	−0.038	0.198	0.041	0.052	0.055	−0.026			
	± 0.007	0.013	0.020	0.020	0.024	0.024	0.025			
1.005	0.193	0.004	0.134	0.004	0.052	0.027	−0.024			
	± 0.007	0.013	0.019	0.021	0.024	0.025	0.027			
1.045	0.161	0.035	0.104	−0.059	−0.030	0.027	−0.047	0.038		
	± 0.005	0.010	0.013	0.014	0.017	0.019	0.020	0.023		
1.085	0.130	0.066	0.066	−0.046	−0.036	0.006	−0.005	−0.010		
	± 0.005	0.010	0.012	0.014	0.016	0.018	0.019	0.020		
1.125	0.130	0.092	0.067	−0.036	−0.063	0.012	−0.031	−0.024		
	± 0.005	0.009	0.011	0.013	0.015	0.017	0.018	0.019		
1.165	0.115	0.111	0.063	−0.044	−0.073	−0.021	−0.035	−0.017		
	± 0.004	0.009	0.009	0.011	0.013	0.015	0.016	0.016		
1.205	0.109	0.099	0.068	−0.061	−0.053	−0.013	−0.020	−0.013		
	± 0.004	0.009	0.009	0.011	0.013	0.015	0.015	0.016		
1.245	0.108	0.103	0.058	−0.070	−0.061	−0.002	0.000	−0.007	0.005	0.047
	± 0.003	0.008	0.008	0.010	0.011	0.013	0.015	0.019	0.017	0.019
1.285	0.094	0.083	0.050	−0.085	−0.068	−0.021	0.022	−0.021	−0.007	−0.023
	± 0.003	0.007	0.007	0.009	0.010	0.012	0.014	0.017	0.015	0.018
1.320	0.085	0.070	0.040	−0.077	−0.042	−0.024	0.029	−0.013	−0.021	−0.019
	± 0.003	0.007	0.008	0.010	0.011	0.012	0.015	0.017	0.016	0.019
1.355	0.115	0.083	0.056	−0.078	−0.020	−0.013	0.085	−0.016	0.008	0.026
	± 0.003	0.007	0.008	0.010	0.011	0.013	0.015	0.017	0.016	0.018

The values of B_l are given in table 10.

The $\bar{K}^0 n$ cross sections were obtained from the total weighted number of events and the microbarn equivalents. The $\bar{K}^0_S$ branching ratio into $\pi^+\pi^-$ was taken to be 0.688 [3]. The cross sections obtained at each energy are given in table 17 and shown in fig. 10(b).

The $\Lambda\pi^0$ cross section was obtained in two ways. In the first method events with a missing mass squared (MM^2) within one standard deviation of m_π^2 were assigned a weight of 1 and events with $|MM^2 - m_\pi^2|$ greater than one standard deviation were given a weight of 2 if $MM^2 < m_\pi^2$, or 0 if $MM^2 > m_\pi^2$. Cross sections obtained in this way are given in table 17 and shown in fig. 10(c). As a check, a maximum likelihood analysis of the Λ + neutrals events was carried out. This analysis attempted to fit the observed MM^2 spectrum, and the Λ production angular distribution for the $\Lambda\pi^0$ channel, assuming the main reactions contributing are $K^-p \to \Lambda\pi^0$, $\Sigma^0\pi^0$, $\Lambda\pi^0\pi^0$, $\Lambda\eta^0$ and $\Sigma^0\eta^0$. The cross sections for these reactions were free to vary in the fit, as were the Legendre expansion coefficients for the $\Lambda\pi^0$ reaction. Results obtained for the $\Lambda\pi^0$ cross sections were in excellent agreement with those from the first method. The $\Sigma^0\pi^0$ cross sections obtained in this analysis are given in table 17 and shown in fig. 10(f).

Table 9
Polarisation distributions for $K^-p \to \Lambda\pi^0$ (given as cos θ bin lower limit, polarisation, errors; the bins are continuous over the complete cos θ range)

0.960 GeV/c			1.005 GeV/c			1.045 GeV/c		
−1.0	0.46	±0.23	−1.0	0.13	±0.25	−1.0	−0.27	±0.24
−0.9	0.28	±0.23	−0.9	0.35	±0.29	−0.9	−0.04	±0.24
−0.8	0.23	±0.25	−0.8	0.41	±0.27	−0.8	0.03	±0.23
−0.7	0.32	±0.28	−0.7	−0.71	±0.30	−0.7	−0.07	±0.33
−0.6	0.88	±0.32	−0.6	0.02	±0.32	−0.6	−0.07	±0.34
−0.5	0.14	±0.34	−0.5	0.18	±0.28	−0.5	−0.08	±0.36
−0.4	0.68	±0.38	−0.3	0.91	±0.39	−0.4	0.42	±0.27
−0.3	0.68	±0.35	−0.2	0.63	±0.36	−0.2	0.49	±0.39
−0.2	1.00	±0.33	−0.1	0.73	±0.29	−0.1	0.92	±0.35
−0.1	1.42	±0.36	0.1	0.76	±0.37	0.0	0.82	±0.33
0.0	1.14	±0.26	0.2	0.50	±0.38	0.1	−0.11	±0.33
0.2	1.00	±0.38	0.3	0.57	±0.39	0.2	0.50	±0.33
0.3	0.78	±0.39	0.4	−0.68	±0.39	0.3	0.13	±0.34
0.4	0.00	±0.42	0.5	−0.05	±0.38	0.4	0.50	±0.29
0.5	−0.76	±0.28	0.6	−0.76	±0.33	0.5	−0.22	±0.29
0.7	−1.34	±0.24	0.7	−1.14	±0.29	0.6	0.23	±0.27
0.8	−1.24	±0.24	0.8	−1.39	±0.25	0.7	−0.51	±0.26
0.9	−0.86	±0.25	0.9	−0.85	±0.26	0.8	−0.90	±0.24
						0.9	−1.13	±0.23
1.085 GeV/c			1.125 GeV/c			1.165 GeV/c		
−1.0	−0.73	±0.28	−1.0	0.58	±0.39	−1.0	−0.75	±0.38
−0.9	−0.64	±0.28	−0.9	−0.50	±0.32	−0.9	−0.47	±0.37
−0.8	−0.33	±0.31	−0.8	−0.44	±0.31	−0.8	−0.79	±0.35
−0.7	0.16	±0.35	−0.7	−0.06	±0.38	−0.7	−0.03	±0.34
−0.6	−0.13	±0.38	−0.6	0.18	±0.39	−0.5	−0.66	±0.36
−0.5	0.95	±0.30	−0.5	0.33	±0.35	−0.3	0.39	±0.40
−0.3	0.38	±0.33	−0.3	0.23	±0.34	−0.1	0.41	±0.31
−0.1	0.57	±0.29	−0.1	0.36	±0.30	0.1	0.46	±0.40
0.1	0.40	±0.37	0.1	−0.16	±0.36	0.2	1.08	±0.30
0.2	0.21	±0.35	0.2	0.36	±0.30	0.3	0.52	±0.31
0.3	0.47	±0.31	0.3	0.21	±0.32	0.4	0.26	±0.27
0.4	0.29	±0.27	0.4	0.43	±0.28	0.5	−0.01	±0.25
0.5	0.08	±0.29	0.5	0.24	±0.29	0.6	−0.26	±0.25
0.6	−0.54	±0.25	0.6	0.44	±0.25	0.7	−0.22	±0.23
0.7	−0.74	±0.26	0.7	−0.40	±0.25	0.8	−0.68	±0.23
0.8	−0.74	±0.26	0.8	−0.67	±0.24	0.9	−1.02	±0.26
0.9	−0.62	±0.29	0.9	−1.12	±0.23			

6. The reactions $K^-p \to \Sigma^\pm\pi^\mp$

Events of topology 210 were fitted to hypotheses involving the decay of $\Sigma^\pm$, K and, at higher momenta, Ξ^-. This resulted in a cleanly separated sample of $\Sigma^\pm\pi^\mp$

Table 9 (continued)

1.205 GeV/*c*			1.245 GeV/*c*			1.285 GeV/*c*		
−1.0	0.06	±0.38	−1.0	0.06	±0.34	−1.0	0.14	±0.32
−0.9	−0.71	±0.37	−0.9	−0.25	±0.33	−0.9	0.39	±0.38
−0.8	−0.15	±0.41	−0.8	−0.50	±0.38	−0.8	−0.45	±0.37
−0.7	−0.35	±0.33	−0.7	−0.13	±0.36	−0.7	−0.81	±0.30
−0.5	0.21	±0.38	−0.6	−0.87	±0.31	−0.5	0.17	±0.39
−0.2	0.60	±0.39	−0.4	−0.18	±0.36	−0.3	1.07	±0.34
0.0	0.68	±0.39	−0.1	0.25	±0.30	0.0	0.50	±0.34
0.1	0.42	±0.39	0.1	0.89	±0.33	0.1	0.67	±0.38
0.2	0.27	±0.35	0.2	0.29	±0.28	0.2	0.45	±0.33
0.3	0.62	±0.31	0.3	0.47	±0.27	0.3	0.39	±0.26
0.4	0.71	±0.30	0.4	0.63	±0.25	0.4	0.54	±0.24
0.5	0.38	±0.26	0.5	0.41	±0.22	0.5	−0.05	±0.23
0.6	−0.14	±0.24	0.6	0.29	±0.22	0.6	−0.07	±0.23
0.7	−0.14	±0.24	0.7	−0.19	±0.22	0.7	0.05	±0.23
0.8	−0.40	±0.25	0.8	0.02	±0.23	0.8	−0.89	±0.23
0.9	−0.86	±0.28	0.9	−0.17	±0.27	0.9	−0.19	±0.33

1.320 GeV/*c*			1.355 GeV/*c*		
−1.0	0.70	±0.30	−1.0	−0.17	±0.24
−0.9	0.51	±0.39	−0.9	0.49	±0.37
−0.8	−0.66	±0.30	−0.8	−0.47	±0.40
−0.6	−0.35	±0.33	−0.7	−1.25	±0.33
−0.4	−0.20	±0.37	−0.6	−0.41	±0.34
−0.2	0.70	±0.36	−0.5	−0.76	±0.39
0.0	0.31	±0.41	−0.4	−0.19	±0.39
0.1	0.12	±0.34	−0.3	0.59	±0.33
0.2	0.10	±0.34	−0.1	−0.07	±0.30
0.3	−0.20	±0.26	0.1	−0.04	±0.30
0.4	0.13	±0.24	0.2	0.03	±0.28
0.5	0.38	±0.23	0.3	−0.01	±0.23
0.6	0.18	±0.26	0.4	−0.28	±0.23
0.7	−0.43	±0.23	0.5	0.34	±0.22
0.8	−0.12	±0.26	0.6	0.18	±0.21
0.9	−0.47	±0.27	0.7	0.47	±0.23
			0.8	0.10	±0.25
			0.9	−0.09	±0.24

reactions. The differential and total cross section results presented here were obtained using the events where the Σ decays by $\Sigma^{\pm} \to \pi^{\pm} n$. The events with the Σ^+ decay $\Sigma^+ \to p\pi^0$ were only used to obtain polarisation information. The usual beam checks were applied to all events and in addition the Σ decay vertex was required to be within a restricted fiducial volume.

The biases inherent in this type of event were investigated and corrected as follows:

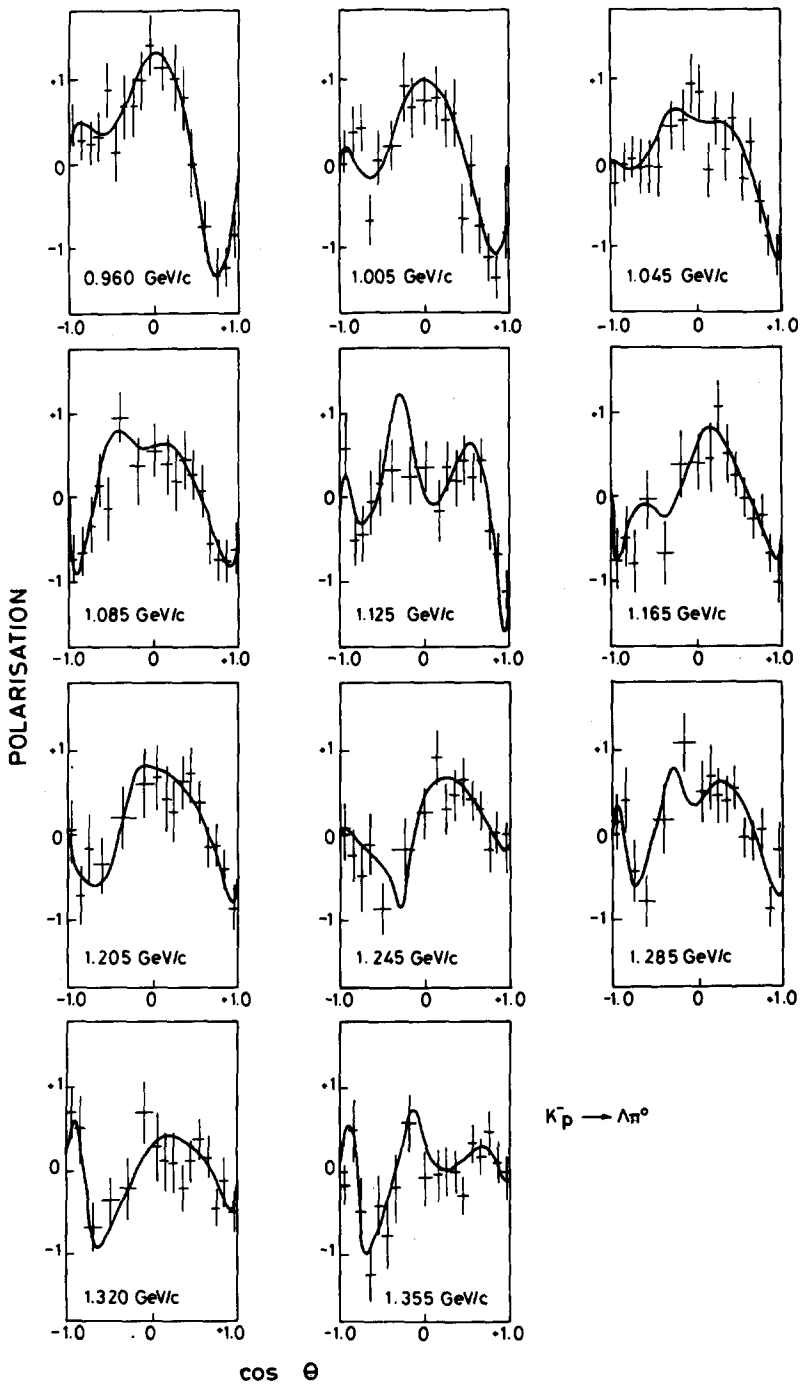

Fig. 6. Polarisation distributions of Λ from $K^-p \to \Lambda\pi^0$. The curves are from fits to $d\sigma/d(\cos\theta)$ and $P\, d\sigma/d(\cos\theta)$ as described.

Table 10
Values of associated Legendre B_l coefficients for $K^-p \to \Lambda\pi^0$

Beam momentum (GeV/c)	B_1	B_2	B_3	B_4	B_5	B_6	B_7
0.960	0.060	−0.101	−0.058	−0.051	0.010	−0.003	
	± 0.015	0.014	0.012	0.011	0.010	0.010	
1.005	0.027	−0.048	−0.080	−0.041	0.003	−0.011	
	± 0.018	0.015	0.013	0.012	0.011	0.011	
1.045	0.015	−0.027	−0.052	−0.032	−0.020	−0.010	
	± 0.014	0.012	0.010	0.009	0.008	0.008	
1.085	0.019	−0.021	−0.049	−0.010	−0.021	0.009	
	± 0.014	0.012	0.010	0.009	0.008	0.008	
1.125	0.017	−0.011	−0.035	−0.033	−0.039	−0.030	
	± 0.013	0.011	0.009	0.008	0.007	0.007	
1.165	−0.010	−0.005	−0.038	−0.026	−0.012	0.004	
	± 0.011	0.010	0.008	0.007	0.006	0.006	
1.205	0.017	0.006	−0.036	−0.022	−0.012	−0.005	
	± 0.011	0.009	0.008	0.007	0.006	0.006	
1.245	0.031	0.025	−0.007	−0.019	−0.006	0.001	0.002
	± 0.010	0.009	0.007	0.006	0.006	0.005	0.005
1.285	0.019	0.005	−0.020	−0.021	−0.010	−0.005	0.008
	± 0.009	0.008	0.006	0.005	0.005	0.005	0.004
1.320	0.008	0.007	−0.009	−0.018	0.000	−0.005	0.004
	± 0.009	0.008	0.006	0.006	0.005	0.005	0.004
1.355	0.011	0.016	0.002	−0.006	0.005	−0.015	0.000
	± 0.009	0.008	0.006	0.006	0.005	0.005	0.005

(a) *Decay angle and slow decay pion losses.* Events with small projected decay angle in the xy plane are often missed, as are events with a slow charged pion from the Σ decay. Both these losses are evident in the distributions of ϕ and $\cos\delta$, where

Table 11
The Σ decay angle cuts

Σ momentum bin (GeV/c)	ϕ_c/π	$1 - \cos\delta_1$	
		$\Sigma^-\pi^+$	$\Sigma^+_\pi\pi^-$
0.0–0.2	0.0	0.0	0.0
0.2–0.4	0.0	0.0	0.0
0.4–0.6	0.0	0.0	0.0
0.6–0.8	0.02	0.05	0.0
0.8–1.0	0.04	0.05	0.10
1.0–1.2	0.04	0.05	0.10
1.2–1.4	0.04	0.15	0.15
1.4–2.0	0.06	0.15	0.15

Table 12
(a) The $K^-p \to \Sigma^-\pi^+$ events

Beam momentum (GeV/c)	No. after beam and vertex cuts	No. after all cuts	Final weighted no.	Average W_A	Average life-time weight	Average total weight
0.960	691	621	936 ± 38	1.09	1.16	1.51
1.005	706	599	870 ± 36	1.10	1.16	1.45
1.045	1193	1043	1582 ± 49	1.11	1.17	1.52
1.085	1136	979	1466 ± 47	1.10	1.17	1.50
1.125	1156	1004	1475 ± 47	1.11	1.17	1.47
1.165	1074	952	1397 ± 45	1.10	1.18	1.47
1.205	908	793	1182 ± 42	1.10	1.19	1.49
1.245	924	802	1190 ± 42	1.10	1.18	1.48
1.285	751	631	969 ± 39	1.09	1.21	1.53
1.320	552	481	735 ± 33	1.09	1.21	1.53
1.355	741	651	1002 ± 39	1.10	1.21	1.54

(b) The $K^-p \to \Sigma^+\pi^-$, $\Sigma^+ \to \pi^+n$ events

0.960	435	350	635 ± 34	1.05	1.38	1.82
1.005	430	345	596 ± 32	1.06	1.39	1.73
1.045	739	598	1082 ± 45	1.07	1.39	1.81
1.085	594	474	845 ± 39	1.07	1.43	1.78
1.125	593	478	865 ± 40	1.06	1.46	1.81
1.165	648	526	936 ± 42	1.07	1.45	1.78
1.205	648	524	956 ± 42	1.08	1.43	1.83
1.245	818	664	1193 ± 47	1.09	1.42	1.80
1.285	957	758	1367 ± 51	1.09	1.44	1.80
1.320	697	564	1031 ± 44	1.09	1.44	1.83
1.355	1073	868	1562 ± 54	1.10	1.41	1.80

ϕ is the angle between the normal to the decay plane and an event dependent polar axis in the direction $\hat{\Sigma} \times (\hat{\Sigma} \times \hat{z})$ (where $\hat{\Sigma}$ is a unit vector in the direction of the Σ lab momentum, $\hat{z}$ is as defined in sect. 4 and δ is the angle between $\hat{\Sigma}$ and the decay pion in the Σ rest frame). In the absence of any losses this distribution is expected to be isotropic. Losses are observed around $\phi = \frac{1}{2}\pi$ and $\cos\delta = \pm 1$. The ϕ distributions were inspected in 200 MeV/c intervals of Σ momentum and a cut was applied to each distribution. The $\cos\delta$ distributions of the remaining events were inspected and cut in the same manner. No losses of this type were found when the Σ momentum was less than 600 MeV/c. Events with decay pion momentum less than 40 MeV/c were removed. The decay angle weight applied to the remaining events was:

$$W_A = \left[\frac{1}{2}\left(1 - \frac{2\phi_c}{\pi}\right)(\cos\delta_1 - \cos\delta_2)\right]^{-1}, \tag{16}$$

where $\cos\delta_1$ is the $\cos\delta$ cut corresponding to small forward decay angle losses and

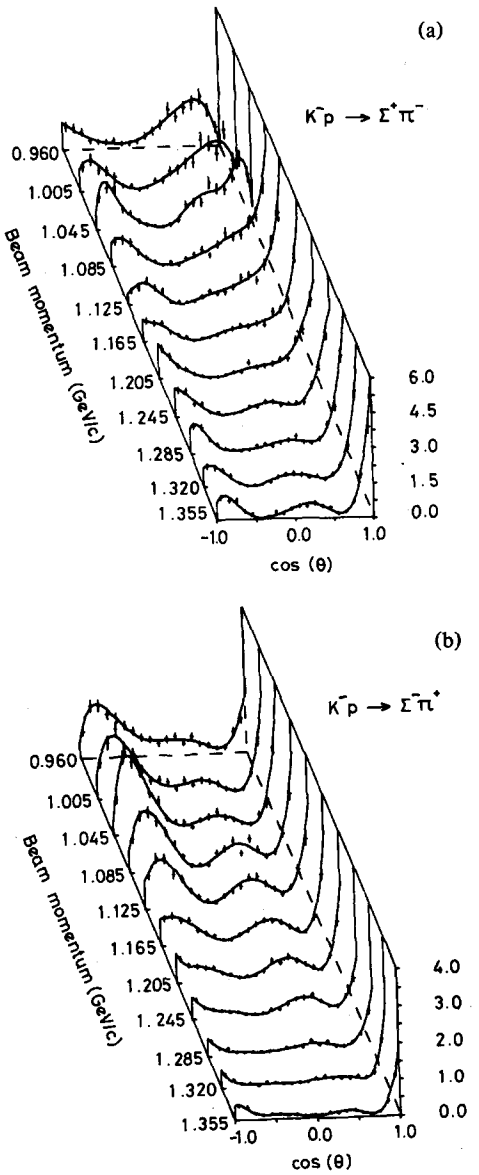

Fig. 7. Differential cross sections for (a) $K^-p \rightarrow \Sigma^-\pi^+$, (b) $K^-p \rightarrow \Sigma^-\pi^+$. The curves are the results of the Legendre polynomial fits described. Vertical axis is $d\sigma/d(\cos\theta)$ in mb/unit $\cos\theta$.

$\cos\delta_2$ the value corresponding to 40 MeV/c decay pion cut (set to -1.0 when the Σ momentum is such that the decay pion momentum is always greater than 40 MeV/c The region cut from the azimuthal angle distribution lies between $\frac{1}{2}\pi \pm \phi_c$. The cuts are given in table 11.

Table 13
Differential cross sections $d\sigma/d(\cos\theta)$ (mb/unit $\cos\theta$)
(a) $K^-p \to \Sigma^-\pi^+$

$\cos\theta$ bin centre		Beam momentum (GeV/c)										
		0.960	1.005	1.045	1.085	1.125	1.165	1.205	1.245	1.285	1.320	1.355
−0.950		0.73	1.01	0.98	0.91	0.92	0.74	0.67	0.53	0.42	0.37	0.39
	±	0.12	0.15	0.12	0.12	0.11	0.09	0.09	0.07	0.06	0.06	0.05
−0.850		1.43	1.54	2.15	1.54	1.39	0.83	0.49	0.33	0.20	0.21	0.35
	±	0.17	0.19	0.18	0.16	0.14	0.10	0.07	0.05	0.04	0.05	0.05
−0.750		1.44	1.90	2.01	1.63	1.37	0.70	0.43	0.26	0.22	0.10	0.17
	±	0.17	0.21	0.18	0.16	0.14	0.09	0.07	0.05	0.04	0.03	0.03
−0.650		1.20	1.36	1.76	1.36	0.94	0.70	0.38	0.23	0.10	0.12	0.12
	±	0.16	0.17	0.16	0.15	0.11	0.09	0.06	0.04	0.03	0.03	0.03
−0.550		1.06	1.20	1.14	1.07	0.82	0.41	0.39	0.21	0.08	0.06	0.15
	±	0.15	0.16	0.13	0.13	0.11	0.07	0.06	0.04	0.03	0.02	0.03
−0.450		0.84	0.78	0.92	0.75	0.49	0.31	0.24	0.17	0.10	0.15	0.14
	±	0.13	0.13	0.12	0.11	0.08	0.06	0.05	0.04	0.03	0.04	0.03
−0.350		0.69	0.47	0.43	0.42	0.30	0.25	0.20	0.09	0.10	0.11	0.10
	±	0.12	0.10	0.08	0.08	0.06	0.05	0.05	0.03	0.03	0.03	0.03
−0.250		0.51	0.47	0.34	0.14	0.19	0.13	0.09	0.10	0.09	0.07	0.12
	±	0.10	0.10	0.07	0.05	0.05	0.04	0.03	0.03	0.03	0.03	0.03
−0.150		0.45	0.41	0.33	0.17	0.12	0.11	0.12	0.12	0.10	0.08	0.09
	±	0.10	0.10	0.07	0.05	0.04	0.03	0.04	0.03	0.03	0.03	0.02
−0.050		0.31	0.23	0.17	0.14	0.31	0.24	0.16	0.21	0.17	0.10	0.05
	±	0.08	0.07	0.05	0.05	0.06	0.05	0.04	0.04	0.04	0.03	0.02
0.050		0.43	0.45	0.35	0.46	0.43	0.35	0.25	0.20	0.18	0.12	0.10
	±	0.09	0.10	0.07	0.08	0.08	0.06	0.05	0.04	0.04	0.03	0.02
0.150		0.52	0.31	0.44	0.57	0.54	0.51	0.54	0.34	0.18	0.20	0.15
	±	0.10	0.08	0.08	0.09	0.09	0.07	0.07	0.05	0.04	0.04	0.03
0.250		0.32	0.42	0.58	0.77	0.78	0.64	0.46	0.47	0.33	0.26	0.13
	±	0.08	0.10	0.09	0.11	0.10	0.08	0.07	0.06	0.05	0.05	0.03
0.350		0.49	0.38	0.42	0.42	0.80	0.58	0.62	0.51	0.24	0.20	0.18
	±	0.10	0.09	0.08	0.08	0.10	0.08	0.08	0.07	0.04	0.04	0.03
0.450		0.29	0.32	0.33	0.81	0.60	0.53	0.50	0.57	0.32	0.20	0.19
	±	0.08	0.09	0.07	0.11	0.09	0.07	0.07	0.07	0.05	0.04	0.03
0.550		0.24	0.18	0.24	0.52	0.45	0.41	0.41	0.40	0.19	0.19	0.12
	±	0.07	0.06	0.06	0.09	0.08	0.07	0.07	0.06	0.04	0.04	0.03
0.650		0.15	0.12	0.19	0.33	0.29	0.34	0.30	0.27	0.19	0.24	0.09
	±	0.06	0.05	0.05	0.07	0.06	0.06	0.06	0.05	0.04	0.05	0.02
0.750		0.16	0.14	0.45	0.43	0.49	0.29	0.26	0.26	0.27	0.19	0.14
	±	0.06	0.06	0.08	0.08	0.08	0.06	0.05	0.05	0.05	0.04	0.03
0.850		0.58	0.59	0.74	0.92	0.96	0.64	0.62	0.53	0.50	0.32	0.40
	±	0.11	0.12	0.11	0.12	0.12	0.08	0.08	0.07	0.06	0.05	0.05
0.950		0.94	1.52	2.27	2.01	1.76	1.81	1.55	0.99	1.11	1.24	1.13
	±	0.15	0.20	0.20	0.19	0.17	0.15	0.14	0.10	0.10	0.11	0.09

(b) *Lifetime weights.* These are essentially as described in sect. 5(b), using eq. (11) with $\tau_{\Sigma^-} = 1.482 \times 10^{-10}$ sec, $\tau_{\Sigma^+} = 0.800 \times 10^{-10}$ sec and l_2 is set to the potential decay length, l_{max} or $pc\tau_{max}/M$, whichever is the smallest. The limits l_{max} and

Table 13 (continued)
(b) $K^-p \to \Sigma^+\pi^-$

cos θ bin centre		Beam momentum (GeV/c)										
		0.960	1.005	1.045	1.085	1.125	1.165	1.205	1.245	1.285	1.320	1.355
−0.950		1.03	1.11	1.41	1.10	0.59	0.89	1.31	1.16	1.20	0.90	0.97
	±	0.22	0.24	0.22	0.19	0.14	0.15	0.18	0.15	0.15	0.14	0.12
−0.850		0.93	1.41	1.80	1.15	0.71	0.76	0.99	1.11	1.14	0.84	0.81
	±	0.21	0.27	0.25	0.20	0.15	0.14	0.16	0.15	0.14	0.13	0.11
−0.750		0.75	0.94	1.80	1.05	1.00	0.78	0.57	0.54	0.62	0.70	0.83
	±	0.19	0.22	0.25	0.19	0.18	0.14	0.12	0.10	0.11	0.12	0.11
−0.650		0.37	0.88	0.84	0.63	0.69	0.42	0.42	0.55	0.39	0.47	0.35
	±	0.13	0.21	0.17	0.15	0.15	0.10	0.10	0.10	0.08	0.10	0.07
−0.550		0.33	0.62	0.67	0.35	0.57	0.27	0.20	0.15	0.17	0.12	0.24
	±	0.12	0.18	0.15	0.11	0.13	0.08	0.07	0.05	0.05	0.05	0.06
−0.450		0.29	0.21	0.32	0.17	0.06	0.17	0.10	0.15	0.14	0.02	0.04
	±	0.12	0.10	0.11	0.08	0.04	0.06	0.05	0.05	0.05	0.03	0.02
−0.350		0.34	0.21	0.14	0.03	0.09	0.00	0.02	0.02	0.09	0.06	0.09
	±	0.13	0.10	0.07	0.05	0.05	0.03	0.03	0.03	0.04	0.04	0.03
−0.250		0.20	0.05	0.07	0.17	0.03	0.10	0.05	0.06	0.14	0.08	0.29
	±	0.10	0.07	0.05	0.08	0.04	0.05	0.03	0.03	0.05	0.04	0.06
−0.150		0.20	0.11	0.04	0.03	0.06	0.12	0.10	0.15	0.31	0.14	0.21
	±	0.10	0.08	0.05	0.05	0.04	0.06	0.05	0.05	0.07	0.05	0.05
−0.050		0.29	0.38	0.14	0.29	0.26	0.22	0.22	0.36	0.33	0.37	0.44
	±	0.12	0.15	0.07	0.10	0.09	0.07	0.07	0.08	0.07	0.09	0.08
0.050		0.48	0.38	0.34	0.43	0.49	0.32	0.20	0.34	0.24	0.47	0.54
	±	0.15	0.14	0.11	0.13	0.13	0.09	0.07	0.08	0.06	0.10	0.09
0.150		0.70	0.79	0.96	0.65	0.39	0.45	0.63	0.53	0.40	0.52	0.52
	±	0.18	0.21	0.19	0.15	0.11	0.11	0.13	0.10	0.08	0.10	0.09
0.250		0.96	0.88	1.05	0.41	0.42	0.59	0.41	0.53	0.52	0.46	0.64
	±	0.22	0.21	0.19	0.12	0.12	0.12	0.10	0.10	0.10	0.10	0.10
0.350		1.64	1.11	1.05	0.85	0.62	0.56	0.44	0.37	0.67	0.33	0.53
	±	0.29	0.24	0.19	0.17	0.14	0.12	0.10	0.09	0.11	0.08	0.09
0.450		1.33	1.14	1.90	1.34	1.04	0.68	0.53	0.45	0.41	0.37	0.46
	±	0.26	0.25	0.26	0.22	0.18	0.13	0.11	0.09	0.08	0.09	0.08
0.550		1.69	2.12	1.61	1.16	1.13	0.58	0.71	0.48	0.35	0.26	0.20
	±	0.29	0.34	0.24	0.21	0.19	0.12	0.13	0.10	0.08	0.07	0.05
0.650		1.88	1.94	1.57	1.24	0.90	1.14	0.74	0.46	0.51	0.44	0.25
	±	0.31	0.33	0.24	0.21	0.17	0.17	0.14	0.09	0.10	0.10	0.06
0.750		2.16	1.52	2.14	1.74	1.55	1.25	1.55	1.21	1.16	0.87	0.70
	±	0.35	0.31	0.30	0.26	0.23	0.18	0.20	0.16	0.15	0.14	0.10
0.850		1.57	2.50	2.90	2.12	2.50	1.64	1.98	2.03	1.93	1.67	1.87
	±	0.31	0.41	0.36	0.30	0.31	0.22	0.24	0.21	0.20	0.20	0.17
0.950		0.81	1.21	2.19	3.38	3.80	3.64	3.26	3.45	4.13	4.02	3.89
	±	0.24	0.31	0.35	0.42	0.43	0.37	0.35	0.31	0.32	0.34	0.28

τ_{max} correspond to additional cuts applied to the Σ track length and proper lifetime, with $l_{max} = 20$ cms and $\tau_{max} = 4\tau_\Sigma$ (p and M are the Σ momentum and mass respectively). The minimum projected length cut was chosen to be 0.3 cm., the mi-

Table 14
Values of Legendre A_l coefficients (with $A_0 = \sigma/4\pi\lambda^2$)

(a) $K^-p \to \Sigma^-\pi^+$

Beam momentum (GeV/c)	A_0	A_1	A_2	A_3	A_4	A_5	A_6	A_7	A_8
0.960	0.067	−0.047	0.041	0.035	−0.012	0.053	−0.004		
	± 0.004	0.006	0.007	0.008	0.009	0.010	0.011		
1.005	0.078	−0.055	0.078	0.057	−0.004	0.110	−0.003		
	± 0.004	0.007	0.009	0.010	0.011	0.013	0.013		
1.045	0.097	−0.050	0.122	0.078	−0.002	0.159	−0.012	0.027	
	± 0.004	0.007	0.009	0.010	0.011	0.013	0.013	0.014	
1.085	0.097	−0.020	0.101	0.044	−0.010	0.135	0.012	−0.023	
	± 0.004	0.007	0.009	0.010	0.011	0.012	0.013	0.013	
1.125	0.093	−0.008	0.094	0.016	0.016	0.116	0.002	−0.025	
	± 0.004	0.006	0.008	0.009	0.010	0.012	0.012	0.013	
1.165	0.073	0.015	0.077	0.021	0.046	0.102	0.030	−0.009	
	± 0.003	0.005	0.007	0.008	0.009	0.010	0.011	0.011	
1.205	0.063	0.027	0.066	0.017	0.057	0.088	0.062	0.013	
	± 0.003	0.005	0.007	0.008	0.009	0.010	0.011	0.011	
1.245	0.052	0.027	0.041	−0.010	0.037	0.053	0.035	−0.001	−0.020
	± 0.002	0.004	0.005	0.006	0.007	0.007	0.008	0.008	0.008
1.285	0.041	0.031	0.051	0.017	0.053	0.037	0.028	0.002	−0.000
	± 0.002	0.004	0.005	0.006	0.007	0.007	0.008	0.008	0.008
1.320	0.038	0.031	0.054	0.025	0.057	0.039	0.036	0.015	−0.002
	± 0.002	0.004	0.005	0.006	0.007	0.008	0.008	0.009	0.009
1.355	0.037	0.020	0.063	0.033	0.059	0.044	0.036	0.022	−0.006
	± 0.002	0.003	0.005	0.006	0.006	0.007	0.007	0.008	0.008

(b) $K^-p \to \Sigma^+\pi^-$

0.960	0.094	0.068	0.054	−0.094	−0.068	−0.024	−0.007		
	± 0.006	0.010	0.012	0.014	0.016	0.018	0.019		
1.005	0.110	0.068	0.103	−0.073	−0.075	0.006	−0.037		
	± 0.007	0.013	0.015	0.017	0.019	0.021	0.024		
1.045	0.137	0.079	0.167	−0.061	−0.059	0.043	−0.041	−0.047	
	± 0.007	0.012	0.015	0.017	0.019	0.022	0.024	0.025	
1.085	0.115	0.101	0.170	0.013	0.011	0.060	−0.033	−0.017	
	± 0.006	0.013	0.016	0.018	0.019	0.021	0.022	0.023	
1.125	0.112	0.124	0.185	0.076	0.036	0.081	0.001	−0.043	
	± 0.006	0.013	0.016	0.018	0.020	0.022	0.024	0.026	
1.165	0.102	0.104	0.177	0.060	0.076	0.087	0.003	0.008	
	± 0.005	0.011	0.015	0.016	0.018	0.020	0.021	0.022	
1.205	0.106	0.098	0.205	0.039	0.091	0.042	−0.014	−0.029	
	± 0.005	0.011	0.016	0.017	0.019	0.020	0.022	0.023	
1.245	0.108	0.093	0.209	0.075	0.127	0.091	−0.023	−0.022	−0.030
	± 0.005	0.010	0.015	0.016	0.018	0.019	0.021	0.023	0.024
1.285	0.119	0.108	0.238	0.102	0.171	0.109	0.012	0.009	−0.025
	± 0.005	0.011	0.016	0.017	0.019	0.021	0.022	0.024	0.026
1.320	0.109	0.107	0.222	0.120	0.182	0.140	0.021	0.007	0.036
	± 0.005	0.012	0.017	0.018	0.021	0.023	0.024	0.025	0.027
1.355	0.120	0.104	0.211	0.125	0.194	0.159	0.004	−0.020	−0.027
	± 0.005	0.010	0.014	0.016	0.018	0.019	0.020	0.022	0.023

nimum value at which the total weighted number of events became independent of the position of the cut. For Σ's with production momenta less than 500 MeV/c or with ranges less than the potential length the weighting factor of eq. (11) was modified for slowing effects. The lifetime distributions were checked with the final cuts imposed and found to be in excellent agreement with those predicted from the world average lifetimes [3]. The effects of the cuts and average values of the weights are summarized in table 12.

The weighted numbers of events were corrected for scanning and throughput efficiencies. The latter, typically in the region of 85–90% with an error of 3%, were calculated for the $\Sigma^-\pi^+$ and for $\Sigma^+\pi^-$ channels separately. The cross sections were calculated using the microbarn equivalents and assuming a branching ratio for the observed decay modes of 1.0 for Σ^- and 0.484 for Σ^+ [3]. The cross sections are given in table 17 and shown in fig. 10(d) and (e), together with other published data. Below 1.1 GeV/c the cross sections reported here are significantly higher than those published in refs. [5] and [6] but at the lowest energies they are in good agreement with the recent results of Jones et al. [7]. These results have been checked extensi-

Table 15
Values of associated Legendre B_l coefficients for $K^-p \to \Sigma^+\pi^-$

Beam momentum (GeV/c)	B_1	B_2	B_3	B_4	B_5	B_6	B_7	B_8
0.960	−0.058	−0.082	−0.013	−0.007	0.006	0.003		
	± 0.009	0.007	0.006	0.006	0.005	0.005		
1.005	−0.051	−0.094	0.001	−0.014	0.010	0.005		
	± 0.009	0.009	0.008	0.006	0.006	0.006		
1.045	−0.036	−0.102	−0.020	−0.042	−0.001	−0.015	−0.002	−0.004
	± 0.009	0.009	0.008	0.007	0.006	0.006	0.006	0.006
1.085	−0.044	−0.074	−0.036	−0.039	0.005	−0.006	−0.007	−0.002
	± 0.008	0.008	0.007	0.007	0.007	0.006	0.007	0.006
1.125	−0.023	−0.045	−0.045	−0.039	−0.017	−0.006	−0.004	0.002
	± 0.009	0.009	0.008	0.007	0.008	0.007	0.010	0.008
1.165	−0.011	−0.033	−0.049	−0.031	−0.005	0.002	−0.016	0.005
	± 0.007	0.007	0.006	0.006	0.006	0.006	0.007	0.005
1.205	−0.023	−0.037	−0.051	−0.028	−0.025	0.003	−0.008	0.004
	± 0.008	0.008	0.008	0.007	0.008	0.006	0.007	0.007
1.245	−0.006	−0.022	−0.040	−0.022	−0.013	0.003	0.003	0.001
	± 0.007	0.007	0.007	0.006	0.005	0.005	0.004	0.004
1.285	0.012	−0.024	−0.044	−0.034	−0.024	0.005	−0.002	−0.005
	± 0.007	0.007	0.007	0.006	0.006	0.005	0.004	0.005
1.320	0.014	−0.016	−0.026	−0.027	0.000	0.000	0.005	0.000
	± 0.007	0.007	0.007	0.006	0.006	0.005	0.005	0.005
1.355	0.018	−0.015	−0.010	−0.018	−0.008	0.012	−0.001	0.008
	± 0.007	0.006	0.007	0.006	0.005	0.005	0.004	0.004

Table 16
Polarisation distribution from $K^- p \to \Sigma^+ \pi^-$ (given as cos θ bin lower limit, polarisation, error; the bins are continuous over the complete cos θ range)

0.960 GeV/c			1.005 GeV/c			1.045 GeV/c		
−1.0	0.63	±0.28	−1.0	0.94	±0.25	−1.0	1.26	±0.27
−0.8	1.10	±0.29	−0.8	1.03	±0.26	−0.9	0.41	±0.30
−0.6	0.76	±0.33	−0.6	0.76	±0.35	−0.8	0.54	±0.26
−0.3	−0.48	±0.38	−0.2	−0.93	±0.33	−0.7	0.90	±0.28
0.1	−0.77	±0.27	0.2	−0.77	±0.32	−0.6	0.54	±0.33
0.3	−1.07	±0.29	0.3	−0.62	±0.33	−0.4	0.46	±0.35
0.4	−0.61	±0.26	0.4	−1.00	±0.26	0.1	0.03	±0.38
0.5	−1.32	±0.23	0.5	−1.34	±0.22	0.2	−0.77	±0.33
0.6	−0.98	±0.21	0.6	−1.05	±0.21	0.3	−0.62	±0.27
0.7	−0.75	±0.29	0.7	−0.60	±0.28	0.4	−0.19	±0.28
0.8	−1.06	±0.23	0.8	−0.90	±0.29	0.5	−0.70	±0.21
			0.9	−0.60	±0.30	0.6	−0.97	±0.21
						0.7	−0.76	±0.21
						0.8	−0.93	±0.17
						0.9	−1.05	±0.19
1.085 GeV/c			1.125 GeV/c			1.165 GeV/c		
−1.0	0.78	±0.32	−1.0	0.18	±0.27	−1.0	−0.82	±0.35
−0.9	0.58	±0.30	−0.8	0.08	±0.37	−0.9	0.59	±0.29
−0.8	0.62	±0.29	−0.7	0.09	±0.37	−0.8	−0.24	±0.36
−0.7	−0.04	±0.36	−0.5	0.25	±0.36	−0.7	−0.19	±0.35
−0.5	0.13	±0.32	0.1	0.52	±0.30	−0.5	1.09	±0.26
0.1	0.06	±0.29	0.3	0.07	±0.29	0.1	0.89	±0.24
0.3	−0.67	±0.31	0.5	−0.47	±0.32	0.3	−0.29	±0.26
0.4	−0.23	±0.36	0.6	−0.51	±0.25	0.5	−0.08	±0.39
0.5	−0.84	±0.28	0.7	−0.97	±0.24	0.6	−0.77	±0.26
0.6	−1.21	±0.22	0.8	−0.99	±0.17	0.7	−0.93	±0.21
0.7	−0.98	±0.20	0.9	−0.39	±0.17	0.8	−0.93	±0.16
0.8	−0.98	±0.18				0.9	−0.49	±0.17
0.9	−0.61	±0.18						
1.205 GeV/c			1.245 GeV/c			1.285 GeV/c		
−1.0	−0.45	±0.29	−1.0	−0.17	±0.23	−1.0	−0.13	±0.25
−0.9	−0.52	±0.32	−0.9	−0.15	±0.29	−0.9	−0.34	±0.23
−0.8	0.52	±0.33	−0.8	−0.21	±0.28	−0.8	0.36	±0.32
−0.7	0.23	±0.38	−0.7	−0.16	±0.38	−0.7	0.67	±0.30
−0.6	0.22	±0.37	−0.6	0.52	±0.35	−0.6	0.45	±0.33
−0.0	0.41	±0.30	−0.4	0.41	±0.34	−0.1	0.87	±0.26
0.3	0.36	±0.30	−0.0	0.75	±0.26	0.1	1.09	±0.32
0.5	−0.60	±0.36	0.2	0.65	±0.35	0.2	1.30	±0.32
0.6	−0.63	±0.31	0.3	0.56	±0.32	0.3	0.77	±0.27
0.7	−0.87	±0.24	0.4	0.26	±0.26	0.4	1.19	±0.32
0.8	−0.91	±0.17	0.6	−0.92	±0.30	0.5	−0.00	±0.38
0.9	−0.56	±0.17	0.7	−1.13	±0.23	0.6	−0.55	±0.30
			0.8	−0.52	±0.19	0.7	−0.95	±0.23
			0.9	−0.22	±0.13	0.8	−0.51	±0.16
						0.9	−0.46	±0.12

Table 16 (continued)

1.320 GeV/c			1.355 GeV/c		
−1.0	0.50	±0.26	−1.0	−0.16	±0.23
−0.9	0.05	±0.29	−0.9	0.06	±0.25
−0.8	0.07	±0.28	−0.8	0.94	±0.24
−0.6	0.34	±0.37	−0.7	0.84	±0.27
−0.2	0.46	±0.33	−0.6	0.46	±0.33
−0.0	1.06	±0.27	−0.4	−0.19	±0.37
0.1	0.38	±0.37	−0.2	0.28	±0.39
0.2	0.93	±0.31	−0.1	0.41	±0.32
0.3	1.03	±0.30	−0.0	−0.15	±0.29
0.4	0.73	±0.28	0.1	0.33	±0.28
0.6	−1.02	±0.32	0.2	0.68	±0.26
0.7	−0.50	±0.27	0.3	0.39	±0.33
0.8	−0.60	±0.18	0.4	1.04	±0.32
0.9	−0.04	±0.13	0.5	−0.13	±0.29
			0.7	−0.60	±0.24
			0.8	−0.16	±0.17
			0.9	−0.16	±0.12

Table 17
Cross sections

Beam momentum (GeV/c)	Channel cross sections (mb)					
	K^-p	$\bar{K}^0n$	$\Lambda\pi^0$	$\Sigma^-\pi^+$	$\Sigma^+\pi^-$	$\Sigma^0\pi^0$
0.960	21.27 ± 0.68	6.35 ± 0.33	3.72 ± 0.18	1.28 ± 0.07	1.79 ± 0.11	0.83 ± 0.09
1.005	21.75 ± 0.73	7.52 ± 0.40	3.42 ± 0.17	1.38 ± 0.07	1.95 ± 0.12	0.92 ± 0.12
1.045	22.22 ± 0.63	8.67 ± 0.40	2.70 ± 0.12	1.62 ± 0.07	2.29 ± 0.11	0.89 ± 0.11
1.085	19.83 ± 0.59	7.84 ± 0.37	2.06 ± 0.12	1.54 ± 0.07	1.83 ± 0.10	0.89 ± 0.11
1.125	17.89 ± 0.49	6.01 ± 0.28	1.96 ± 0.09	1.40 ± 0.06	1.69 ± 0.09	0.60 ± 0.09
1.165	15.39 ± 0.41	4.42 ± 0.21	1.64 ± 0.08	1.05 ± 0.04	1.46 ± 0.08	0.62 ± 0.08
1.205	13.89 ± 0.37	3.40 ± 0.17	1.49 ± 0.07	0.87 ± 0.04	1.44 ± 0.07	0.49 ± 0.07
1.245	12.32 ± 0.29	2.54 ± 0.12	1.41 ± 0.06	0.68 ± 0.03	1.41 ± 0.06	0.41 ± 0.06
1.285	10.96 ± 0.26	2.09 ± 0.10	1.17 ± 0.05	0.51 ± 0.02	1.48 ± 0.06	0.38 ± 0.05
1.320	10.26 ± 0.26	1.77 ± 0.10	1.03 ± 0.05	0.45 ± 0.02	1.31 ± 0.06	0.29 ± 0.04
1.355	9.53 ± 0.21	1.80 ± 0.09	1.34 ± 0.05	0.43 ± 0.02	1.39 ± 0.06	0.33 ± 0.04

vely, in particular by dividing the data into 22 equally spaced beam momentum intervals. The cross section values obtained lie on a smooth interpolation of the values presented here.

The differential cross sections are shown in fig. 7 and given in table 13. The coefficients of the Legendre polynomial expansion of eq. (9) are presented in table 14. These have been obtained by the method of moments in preference to the minimum χ^2 method since the angular distribution is sparcely populated in the region of $\cos\theta = 0$.

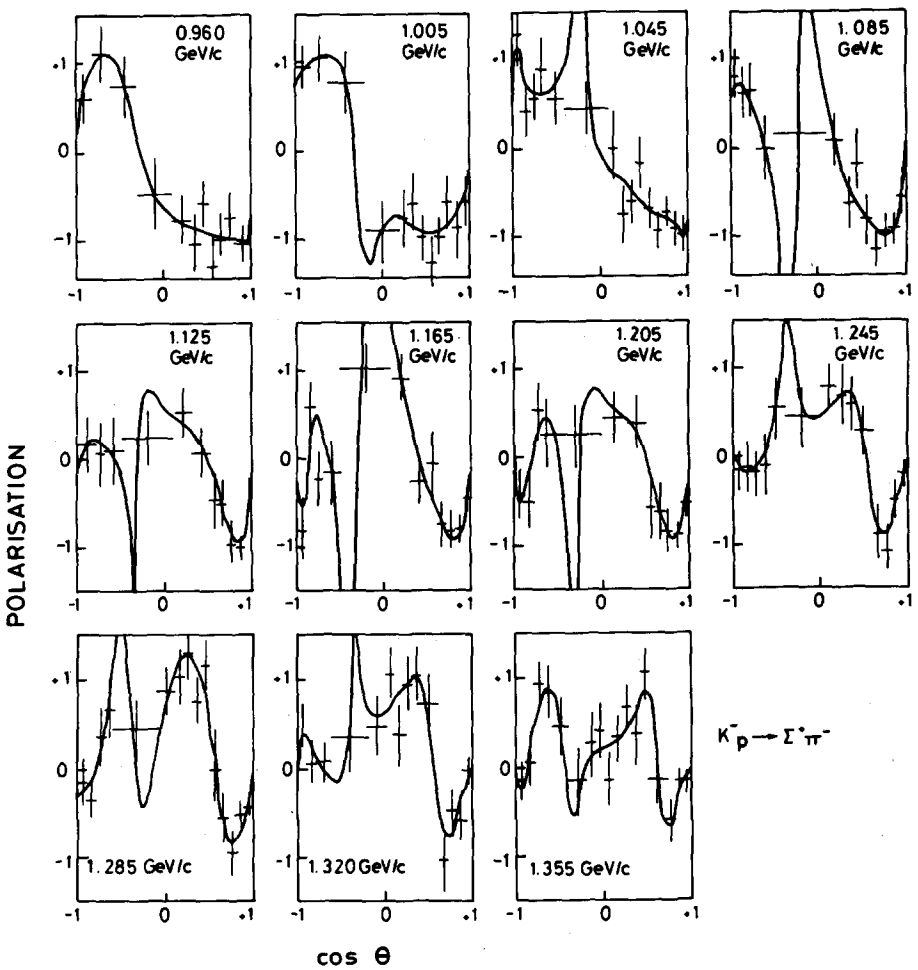

Fig. 8. Polarisation distributions of Σ^+ from $K^-p \to \Sigma^+\pi^-$. The curves are from fits to $d\sigma/d(\cos\theta)$ and $\underset{\sim}{P}\, d\sigma/d(\cos\theta)$ as described.

The Σ polarisation was calculated from all the $\Sigma^+\pi^-$ events with the decay mode $\Sigma^+ \to p\pi^0$. The only cuts applied were the beam cuts, since the biases discussed above do not affect the polarisation determination. The formulation given in sect. 5 was followed except that in eq. (13) α was taken to be -0.979 [3] and $\Sigma_{i=1}^{N}(\cos^2\chi_i)$ was used instead of $\frac{1}{3}N$, as in ref. [8]. The cos θ bins were chosen such that there were at least 20 events in each bin. The distribution $\underset{\sim}{P}\, d\sigma/d(\cos\theta)$, obtained by combining the independently measured $\underset{\sim}{P}$ and $d\sigma/d(\cos\theta)$ distributions, was fitted by an associated Legendre polynomial expansion in the same manner as for reaction (3). The values of B_l are given in table 15. The polarisation distributions are given in table 16 and plotted in fig. 8. The curves shown are the predicted polarisation from

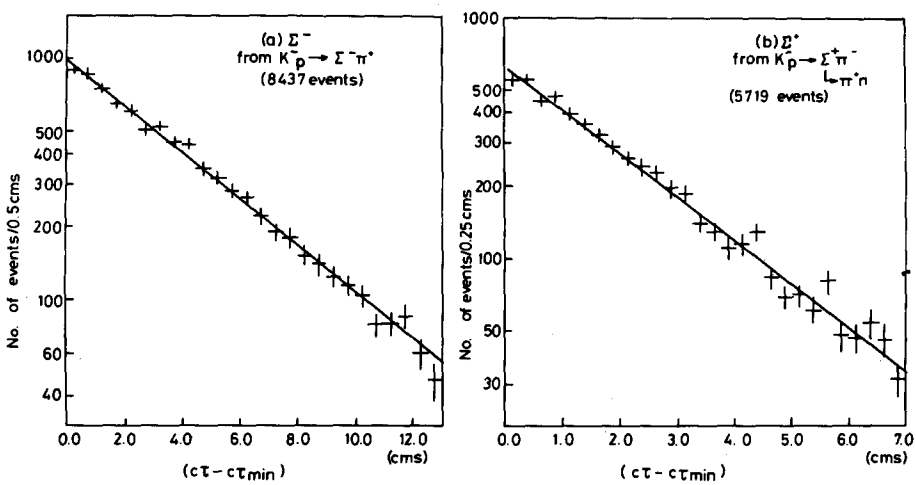

Fig. 9. The lifetime distributions (plotted as $c\tau - c\tau_{min}$) for (a) Σ^-, (b) Σ^+ from $K^-p \to \Sigma^{\mp}\pi^{\pm}$. τ_{min} is the event by event proper lifetime corresponding to the minimum projected length cut imposed. The lines are the results of the maximum likelihood fits described. ($\tau_{\Sigma^-} = 1.49 \times 10^{-10}$ sec, $\tau_{\Sigma^+} = 0.807 \times 10^{-10}$ sec).

the B_l fit to $P\,d\sigma/d(\cos\theta)$ and A_l fit to $d\sigma/d(\cos\theta)$. It should be noted that the polarisation is not fitted directly and in regions where $d\sigma/d(\cos\theta)$ is very small the polarisation is very poorly determined.

The Σ^- and Σ^+ lifetimes have been determined from the $\Sigma^{\pm}\pi^{\mp}$ events using a maximum likelihood method. The cuts and slowing corrections used were as for the lifetime weighting above, but the l_{min} cut was increased to 0.4 cm. The results obtained were $\tau_{\Sigma^-} = (1.49 \pm 0.03) \times 10^{-10}$ sec and $\tau_{\Sigma^+} = (0.807 \pm 0.013) \times 10^{-10}$ sec. The lifetime distributions, plotted as a function of $(c\tau - c\tau_{min})$ where $c\tau_{min}$ is the proper lifetime corresponding to the l_{min} cut for a given event, are shown in fig. 9. The line superimposed corresponds to these results.

7. Conclusions

The results presented here are in general agreement with previous experiments but are of increased accuracy. However, in the case of the $\Sigma^{\pm}\pi^{\mp}$ cross sections some significant discrepancies have been observed. An extensive two-body partial-wave analysis including these data is being carried out and will be published elsewhere.

We would like to thank the CERN 2m bubble chamber crew and the Rutherford Laboratory scanners. We are particularly indebted to Anne Bishop, Pam Coulthard, Jill Cheney and Anne Steer. One of us (RW) wishes to thank the Science Research Council for his studentship.

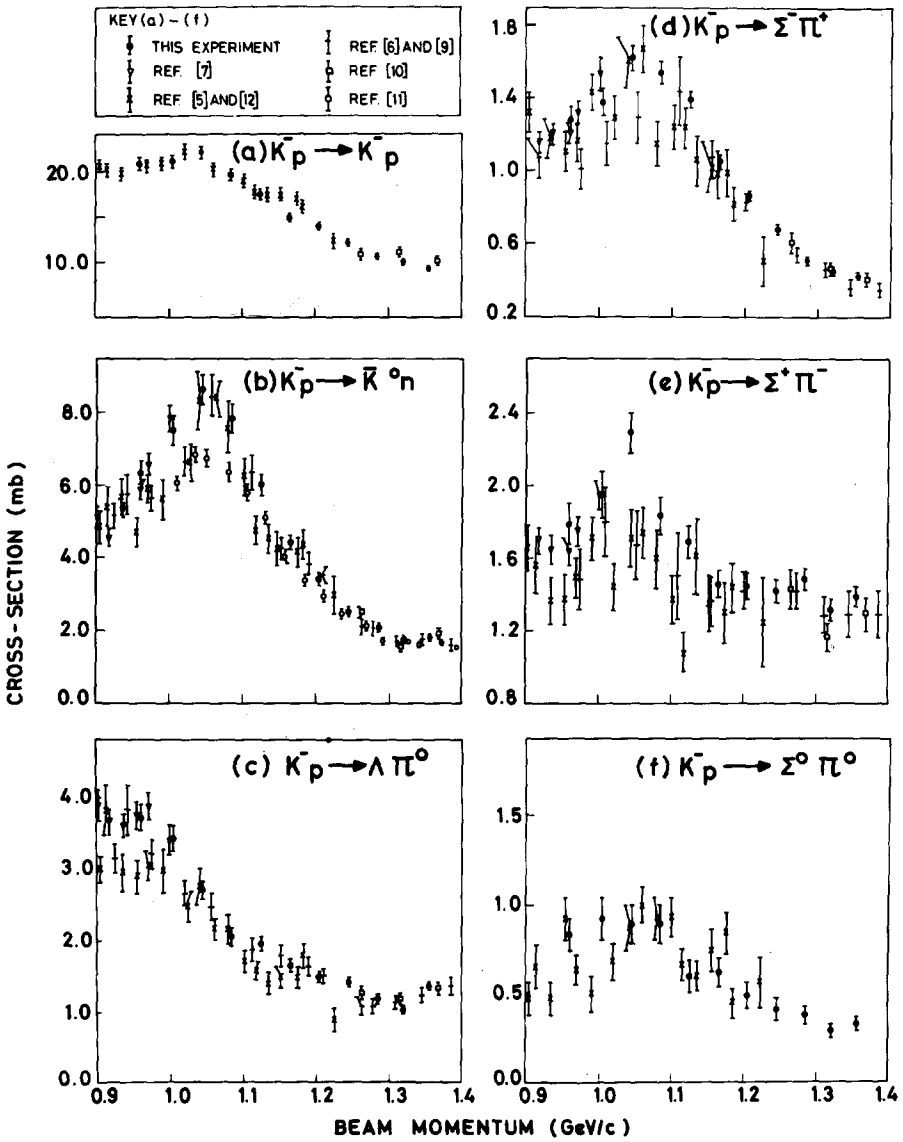

Fig. 10. Channel cross sections. The results of this experiment are plotted together with results from published data. (a) $K^-p \rightarrow K^-p$, (b) $K^-p \rightarrow \bar{K}^0 n$, (c) $K^-p \rightarrow \Lambda\pi^0$, (d) $K^-p \rightarrow \Sigma^-\pi^+$, (e) $K^-p \rightarrow \Sigma^+\pi^-$, (f) $K^-p \rightarrow \Sigma^0\pi^0$.

References

[1] (a) G.P. Gopal, Elastic scattering in K^-p between 0.960 and 1.400 GeV/*c*, Rutherford Laboratory, Bubble Chamber Group Physics Note 65, (1973) unpublished.

(b) A.J. Van Horn, Data reduction and results for $K^-p \to \bar{K}^0 n$ between 0.960 and 1.400 GeV/*c*, Rutherford Laboratory, Bubble Chamber Group Physics Note 87 (1974) unpublished.
(c) E.F. Clayton and R.M. Waters, Data reduction and results for $K^-p \to \Lambda\pi^0$ between 0.960 and 1.400 GeV/*c*, Imperial College, London, Bubble Chamber Group Physics Note (1974) unpublished.
(d) R.T. Ross, The reactions $K^-p \to \Sigma^{\mp}\pi^{\pm}$ between 0.960 and 1.400 GeV/*c*, Rutherford Laboratory, Bubble Chamber Group Physics Note 92 (1975) unpublished.
(c) R.T. Ross and G.P. Gopal, Calculation of cross sections (in particular for $K^-p \to \Sigma^{\mp}\pi^{\pm}$) at 22 momenta from 0.960 to 1.400 GeV/*c*, Rutherford Laboratory, Bubble Chamber Group Physics Note 89 (1975) unpublished.

[2] (a) Geometry Program Manual, Rutherford Laboratory (1968).
(b) Kinematics Program Manual, Rutherford Laboratory (1968).

[3] (a) Particle Data Group, Phys. Letters 50B (1974) 1.
(b) E.F. Clayton, T.C. Bacon, I. Butterworth, R.M. Waters, B. Conforto, G.P. Gopal, G.E. Kalmus, R.T. Ross, A.J. Van Horn, Nucl. Phys. B95 (1975) 130.

[5] R. Armenteros, M. Ferro-Luzzi, D.W.G.S. Leith, R. Levi Setti, A. Minten, R.D. Tripp, H. Filthuth, V. Hepp, E. Kluge, H. Schneider, R. Barloutaud, P. Granet, J. Meyer and J.P. Porte, Nucl. Phys. B8 (1968) 233.

[6] D.F. Kane, Phys. Rev. D5 (1972) 1583.

[7] M. Jones, R. Levi-Setti, D. Merrill and R.D. Tripp, Nucl. Phys. B90 (1975) 349.

[8] R.O. Bangerter, Non-leptonic decay of sigma hyperons, Ph.D. thesis, Lawrence Radiation Laboratory report UCRL-19244 (1969).

[9] A.J. Van Horn, R.P. Ely and J. Louie, Phys. Rev. D6 (1972) 1275.

[10] A. De Bellefon, A. Berthon, L.K. Rangan, J. Vrana, T.C. Bacon, A. Brandstetter, I. Butterworth, S.M. Deen, C.M. Fisher, P.J. Litchfield, R.J. Miller, J.R. Smith, G. Burgun, J. Meyer, E. Pauli, G. Poulard, B. Tallini, W. Wojcik, J. Zatz and R. Strub, Nuovo Cimento 7A (1972) 567.

[11] C. Bricman, M. Ferro-Luzzi, J-M. Perreau, G. Bizard, Y. Déclais, J. Duchon, J. Seguinot and G. Valladas, Phys. Letters 31B (1970) 148.

[12] B. Conforto, D.-M. Harmsen, T. Lasinski, R. Levi Setti, M. Raymund, E. Burkhardt, H. Filthuth, E. Kluge, H. Oberlack and R.R. Ross, Nucl. Phys. B8 (1968) 265.